2

PL-TR-93-2016
Environmental Research Papers, No. 1119

A NIGHTTIME STRUCTURE MODEL OF ATMOSPHERIC OPTICAL TURBULENCE, C_n^2, DERIVED FROM THERMOSONDE AND HIGH RESOLUTION RAWINSONDE MEASUREMENTS

James H. Brown

26 January 1993

Approved for public release; Distribution unlimited

PHILLIPS LABORATORY
Directorate of Geophysics
AIR FORCE MATERIEL COMMAND
HANSCOM AIR FORCE BASE, MA 01731-3010

"This technical report has been reviewed and is approved for publication"

William Blumberg
Simulations Branch
Branch Chief

Roger VanTassel
Optical Environment Division
Division Director

This report has been reviewed by the ESC Public Affairs Office (PA) and is releasable to the National Technical Information Service (NTIS)

Qualified requestors may obtain additional copies from the Defense Technical Information Center. All others should apply to the National Technical Information Service.

If your address has changed, or if you wish to be removed from the mailing list, or if the addressee is no longer employed by your organization, please notify PL/TSI, Hanscom AFB, MA 01731-5000. This will assist us in maintaining a current mailing list.

Do not return copies of this report unless contractual obligations or notices on a specific document requires that it be returned.

REPORT DOCUMENTATION PAGE

Form Approved
OMB No. 0704-0188

1. AGENCY USE ONLY *(Leave blank)*

2. REPORT DATE
26 January 1993

3. REPORT TYPE AND DATES COVERED
Scientific Interim Jan 91 - Jan 93

4. TITLE AND SUBTITLE
A nighttime structure model of atmospheric optical turbulence, C_n^2, derived from thermosonde and high resolution rawinsonde measurements.

5. FUNDING NUMBERS
PE 63220C
WU S3110501
PR S321 TA 13 WU 01

6. AUTHOR(S)
James H. Brown

7. PERFORMING ORGANIZATION NAME(S) AND ADDRESS(ES)
Phillips Laboratory (GPOS)
29 Randolph Road
Hanscom AFB MA 01731-3010

8. PERFORMING ORGANIZATION REPORT NUMBER
PL-TR-93-2016
ERP, No. 1119

9. SPONSORING/MONITORING AGENCY NAME(S) AND ADDRESS(ES)

10. SPONSORING/MONITORING AGENCY REPORT NUMBER

11. SUPPLEMENTARY NOTES

12a. DISTRIBUTION/AVAILABILITY STATEMENT
Approved for public release; distribution unlimited

12b. DISTRIBUTION CODE

13. ABSTRACT *(Maximum 200 words)*

Data from fifteen thermosonde flights was used to develop a simple nightime structure model of C_n^2. High resolution rawinsondes provide fine scale estimates of atmospheric temperature gradients and variances of wind speed. Non-linear regression applied between the thermosonde and rawinsonde measurements provides the model C_n^2 estimator. This quasi-empirical model is based upon the theoretical description given by Tatarski and upon an exponentially scaled estimate of a theoretical model of the eddy dissipation rate given by Weinstock. A discussion of previous models and a comparison with the Dewan et al. microshear model is presented. Model profiles computed for other sites and seasons are compared favorably to related thermosonde profiles.

14. SUBJECT TERMS
Atmospheric structure, Thermosonde, Rawinsonde, C_n^2, Optical turbulence, Turbulence, Outer scale, Temperature fluctuations, Density fluctuations, Radiance variability

15. NUMBER OF PAGES
70

16. PRICE CODE

17. SECURITY CLASSIFICATION OF REPORT	18. SECURITY CLASSIFICATION OF THIS PAGE	19. SECURITY CLASSIFICATION OF ABSTRACT	20. LIMITATION OF ABSTRACT
Unclassified	Unclassified	Unclassified	SAR

Contents

Illustrations

Illustrations

Illustrations

Illustrations

Tables

Acknowledgment

The author gratefully acknowledges the contributions of Neil Grossbard for the computer programs, computer runs, graphics, and insights into the mathematical analysis that helped make this report possible.

A Nighttime Structure Model of Atmospheric Optical Turbulence, C_n^2, Derived from Thermosonde and High Resolution Rawinsonde Measurements

1. INTRODUCTION

It is well known that small fluctuations in atmospheric temperature or density cause fluctuations in the atmospheric index of refraction. These turbulence induced irregularities cause wavefront distortions of optical, infrared, radio, and microwave radiation. Such optical distortions are responsible for random variations of irradiance (scintillation), image blurring, and image distortion. Though these variations are random, statistical averages can be used to describe their effects. Spatial statistics of the random index fluctuations are characterized by structure functions and within the inertial subrange of isotropic turbulence, the structure function is proportional to a power of the spatial separation of the random variable. The constants of proportionality for temperature and refractive index fluctuations are known as C_t^2 and C_n^2 respectively. In describing turbulence effects on optical propagation, C_n^2 is the single most important physical parameter. This report presents an altitude dependent thermosonde derived statistical model for estimating C_n^2 as a function of rawinsonde measured parameters.

Standard balloon borne rawinsondes provide altitude measurements of temperature, pressure, humidity, and winds aloft. High resolution rawinsondes also provide a means for estimating atmospheric temperature gradients and wind speed variances. The Phillips Labortory thermosonde attached to a high resolution rawinsonde provides an estimate of C_t^2 as a function of altitude[1] C_n^2 is evaluated from C_t^2 by the expression $C_n^2 = \left(79.9\times10^{-6}\frac{P}{T^2}\right)^2 C_t^2$. Measurements from over 200 thermosonde flights provide a basis for a simple quasi-empirical rawinsonde model. The model is not fundamental in that neither the first principles convective heat fluxes nor eddy diffusion terms are invoked. Nevertheless, the simplicity of the approach and the statistical agreement with direct measurement warrant consideration.

(Received for Publication 25 January 1993)

[1]Brown, J.H., Good, R.E., Bench, P.M., and Faucher, G., *Sonde Experiments for Comparative Measurements of Optical Turbulence*, AFGL-TR-82-0079, February 1982. ADA118740

2. PREVIOUS MODELS

2.1. Hufnagel Model

Several models of C_n^2 have been introduced into the literature. A survey by Good et al. reviewed the bulk of these up to 1988[2]. Two simple models given by Hufnagel[3] are:

$$C_n^2(\tilde{h}) \propto \tilde{h}^m$$

and,

$$C_n^2(\tilde{h}) = 8.2\times10^{-56}U^2\tilde{h}^{10}e^{-(\tilde{h}/1000)} + 2.7\times10^{-16}e^{-(\tilde{h}/1500)}$$

where, $\tilde{h}$ is meters above sea level, and U is a root-mean-square wind speed averaged over the 5 to 20 km altitude interval. The second of these models is attractive because of the RMS wind speed dependency, which Hufnagel states has a "good correlation" with atmospheric turbulence. Because these models are simple, they do not provide for the thin layering structure of turbulence. Structure could be arranged by introduction of correlated gaussian deviates but the result would be independent of any particular turbulence profile. Also, the model's success in predicting the average C_n^2 measurement as determined by thermosondes often proves unsatisfactory[2].

2.2. NOAA Model

A probabilistic model developed by the Aeronomy Laboratory at NOAA gives C_n^2 in terms of a multivariate probability density function (pdf)[4,5,6]. The independent parameters are N, S, q', and L, which are respectively the Brunt-Vaisala frequency, vertical shear of the horizontal winds, vertical gradient of the specific humidity, and the outer scale of the inertial subrange. The reduced model for a dry atmosphere is given by:

$$\overline{C_n^2}(dry) = C_1 M_0^2 \int_{L_{min}}^{L_{max}} dL\, p_L L^{4/3} \int_0^{\infty} dS\, p_S \int_{-\infty}^{S^2 R_{iC}} dN^2 p_N\left(N^2\right)^2$$

---

[2]Good, R.E., et al. (1988) *Atmospheric Models of Optical Turbulence*, SPIE V928 Modeling of the Atmosphere, Rothman, L.S. ed., pp 165-186.

[3]Wolfe, W.L. and Zississ, G.J., editors, "The Infrared Handbook, Chapter 6", Hufnagel, R.E., auth., *Propagation Through Atmospheric Turbulence*. pg. 6-14, Department of the Navy, 1978.

[4]Warnock, J.M. and VanZandt, T.E., (1985) *A Statistical Model to Estimate The Refractivity Turbulence Structure Constant C_n^2 In Free Atmosphere*, NOAA technical memorandum ERL AL-10, Aeronomy Laboratory, NOAA, Environmental Research Laboratories.

[5]VanZandt, T. E., Gage, K. S., and Warnock, J. M., (1981)., *An Improved Model for The Calculation of profiles of C_n^2 and ε In The Free Atmosphere From Background Profiles Of Wind, Temperature, And Humidity*, Proc. 20th Conf. on Radar Meteorology, Nov. 30-Dec 3, Boston, MA, 129-261.

[6]VanZandt, et.al., *Vertical Profiles Of Refractivity Turbulence Structure Constant: Comparison Of Observations By The Sunset Radar With A New Model*, Radio Science, 13,:819-829.

where, $C_1 = 2.8$, $M_0 = C_2 \frac{P}{gT}$, $C_2 \equiv -77.6 \times 10^{-6}$, P ≡ pressure, T ≡ temperature, and where p_L, p_S, and p_N, are respectively the probability distributions of L, S, and N.

At a smoothed resolution of 500m, the NOAA model has been compared[7] very favorably to radar and thermosonde measurements of C_n^2 but its application remains quite complicated. Also the standard deviations of the distributions are determined from certain empirical scaling factors, some of which depend upon location and perhaps measurement resolution. In particular, the constant in the equation giving the distribution of wind shears depends upon "the range of scales important in the onset of turbulence."[8] While recommended for detailed radar and other low resolution measurements, this technique requires further evidence for its applicability toward producing high resolution C_n^2 structure.

2.3. Dewan et al. Model

Another statistical model developed by Dewan, et al.[2,9] expresses C_n^2 in terms of the well know Tatarski relationship[10] $C_n^2 = 2.8M^2L^{4/3}$, where the factor M gives the gradient of the index of refraction, $M = -79 \times 10^{-6} \frac{PN^2}{gT}$. Dewan et al. estimate L through a regression model of the form: $Log_{10}[L(z)] = -1 + \frac{3}{4}Y(z)$ where, $Y(z) = C_1 + C_2 S$, and where S is the shear evaluated at the standard rawinsonde altitude resolution for wind speed of 300m. Very high resolution smoke trail wind shear data (10m) was employed in the regression analysis to evaluate the constants C_1 and C_2. In this case, a layer thickness was assigned to each region where the smoke trail microshears exceeded a critical value (that is the shear necessary to induce turbulence based on the Richardson number equal to 1/4 criterion). In turn these layer thicknesses were related to 300m resolution rawinsonde shears. Results from this model will be compared to a thermosonde deduced model which is developed in the following section. A reduced form of the Dewan et al. model takes the form: $L(z) = 1.5e^{51.15S(z)}$ in the troposphere, and $L(z) = 0.24e^{63.92S(z)}$ in the stratosphere.

2.4. Thermosonde Model

The thermosonde model is developed from the Tatarski expression, $C_n^2 = 2.8M^2L^{4/3}$, in the manner of the previous model, except that the variables governing M are measured in-situ as a function of altitude. That is, $C_n^2(z) = 2.8[M(z)]^2[L(z)]^{\frac{4}{3}}$. In this expression, $M(z) = -79 \times 10^{-6} \frac{P(z)\omega_B^2(z)}{gT(z)}$ where the altitude dependent parameters are: P(z) (ambient pressure in mb), T(z) (ambient temperature in Kelvin), and $\omega_B(z)$ (local Brunt-Vaisala

---

[7]Warnock, J.M., et.al., Comparison Among Clear-Air Radar, Thermosonde and Optical Measurements and Model Estimates of C_n^2 Made in Very Flat Terrain Over Illinois, Middle Atmospheric Program Handbook, Liu, C.H., ed., V28, June.1989

[8]Green, J.L., et. al. *Comparisons of Refractivity Turbulence Estimates from the Flatland VHF Radar with Other Measurement Techniques,* AMS, 24th Conf. on Radar Meterol., Tallahasee FL, March 1989.

[9]Dewan, E.M., Good, R.E., Beland, R., and Brown, J.H., "A Model for C_n^2 (Optical Turbulence) Profiles from Radiosonde Data". PL-TR-93-2043

[10]Tatarski, V. I., (1961) *Wave Propagation in a Turbulent Medium*, McGraw-Hill

frequency). The square of the Brunt-Vaisala frequency is estimated from in-situ temperature measurements by the expression $\omega_B^2(z) = \frac{g}{T(z)}\left(\frac{dT(z)}{dz} + \Gamma\right)$ where Γ is the dry adiabatic lapse rate, 0.0098 K/m. Given these quantities, L was estimated from the thermosonde measurements by the expression:

$L_{thermosonde} = \left(\frac{C_t^2(smooth)}{2.8 \times \left(\frac{T\omega_B^2}{g}\right)^2}\right)^{3/4}$. A sum of the squares minimization between $L_{thermosonde}$ and over two hundred different combinations of rawinsonde local variables and derived variables was employed to find a regression form that yielded the smallest residual error. The variables of most significance resulted from a combination of the local values of the Brunt-Vaisala frequency, wind speed variance, and their averages. In particular, the measurements led to two suitable empirical models given by the following:

Model (1)

$$Log_{10}(L_{model1}) = a_1 + a_2 Log_{10}(\sigma_v^2) + a_3 Log_{10}(\omega_B + a_4)$$

Model (2)

$$Log_{10}(L_{model2}) = b_1 + b_2 Log_{10}\left(\frac{\sigma_v^2}{\overline{\sigma}_v^2}\right) + b_3 Log_{10}\left(\frac{\omega_B + b_4}{\overline{\omega}_B}\right)$$

where σ_v^2 is an estimate of the local wind speed variance and where the overbars denote their averages over the entire troposphere or stratosphere, depending upon the data region (i.e. different sets of coefficients were determined for the two different regions). The estimated quantities of ω_B^2 and σ_v^2 were derived from high resolution rawinsondes by treating the data over 150m altitude intervals. Linear interpolation of the 20m raw data was employed whenever it was necessary to "line up" values at the same altitude levels. Special consideration was given toward estimating ω_B^2 and σ_v^2. In calculating ω_B^2, the smoothed estimate of the temperature gradient, dT/dz, was found by performing a five point running average over the 20 m high resolution rawinsonde temperature and then performing a least squares parabolic fit over 13 consecutive values of the resulting array. The temperature derivative was found from the slope of the estimated parabola near the seventh value used in finding the fit. In calculating σ_v^2, a running average of the LORAN-derived wind speed over 150 m was subtracted from the local values. Then σ_v^2 was estimated by triangular weighting the sum of the squares of the result, that is,

$$\sigma^2_{v,est.} = \frac{\sum\limits_{over\,150m} (v-\bar{v}_{150})^2 \times Weight_{triang}}{\sum\limits_{over\,150m} Weight_{triang}}$$

. Since the Govind[11] filtering process employed to calculate wind speed from the transmitted LORAN time delays produced altitude resolutions much thicker than 20m, some of the low signal contribution to σ_v^2 is noise induced. There appears to exist, however, sufficient strong velocity fluctuation contributions to σ_v^2 and evident tracking between major peaks in σ_v^2 and C_n^2 to warrant use of this parameterization. Furthermore, use of σ_v^2 in the thermosonde model reduces the residual error between measurement and model.

3. ANALYSIS

Fifteen nighttime thermosonde flights were used to calculate the model constants. These were launched from Pennsylvania State University in May 1986. A typical flight (Launch L4007) is characterized in Figure 1. The graph shows three panels, where the left panel contains plots of ambient temperature and humidity, the right panel contains plots of wind speed and direction, and the center panel contains a plot of high resolution C_n^2. Note that the horizontal dashed lines indicate the altitudes of boundary layer temperature and humidity inversions and, higher up, the tropopause. These levels define the troposphere and stratosphere for the purposes of this report. Overdrawn on the C_n^2 plot is a solid smooth curve that shows a simple empirical model for the entire Pennsylvania State University nighttime data set. This model takes the form: $Log_{10}\left[C_n^2(z)\right] = a + bz + cz^2 + d\varepsilon^{\left[-\frac{1}{2}\left(\frac{z-e}{f}\right)^2\right]}$. It will be called the Penn State Empirical Model (PSEM) and it will be used as a visual reference in comparisons with Model (1) and Model (2). The next series of figures (Figures 2-5) depict a case in the development of Model (1). The left panel in Figure 2 shows the L4007 raw (20m) altitude profile of C_t^2 while the middle and right panels compare the smoothed (150m) C_t^2 with C_t^2 derived from Model (1). As should be expected, the model is smoother than the thermosonde data but quantitatively and structurally the agreement is very good. Figure 3 compares L derived from the thermosonde data (left panel) with Model (1) (right panel). Alignment of the peaks is reasonable. Figure 4 shows the altitude profiles of the measured rawinsonde parameters ω_B (left panel) and σ_v (right panel). Fifteen similar profiles of ω_B^2, σ_v^2, and C_t^2 were used to evaluate the coefficients of Model (1) and Model (2). The middle panel of Figure 4 shows the model C_n^2 profile for L4007. This may be compared to the PSEM depicted as the smooth curve overlay and to the raw C_n^2 of Figure 1. Again there is good quantitative agreement between model and the smoothed measurement. A comparison of L derived for Model (1) and the L4007 thermosonde derived measurement of L is shown in the scatter plot of figure 5. The left and right panels are for tropospheric and stratospheric data respectively. A 45 degree line on these plots indicates exact agreement. The range of variation of L is shown to be wider in the troposphere than in the stratosphere, nevertheless, the data tends to fall about the 45 degree slope. Other individual cases are presented later in this report for comparison. Figure 6 presents a comparison of L derived for Model (1) and all fifteen thermosonde profile derived measurements of L. Figure 7 does the same for Model (2). Here the x's depict the median of the binned data and the error bars depict the standard deviations. Numbers above the error bars indicate the number of points in the bin and

[11]Govind, P.K., (1975) Omega Windfinding Systems, *J. Appl. Meteor.*, V14: 1503-1515

numbers above the plots indicate how many points lay outside three standard deviations. Again the data tend to fall about the 45 degree slope.

As evaluated from the regression analysis, the constants and their standard deviations for Model (1) and Model (2) are given in Table 1.

Table 1. Regression

Constants for Model (1) and Model (2)					
	Model (1)			Model (2)	
	Troposphere	Stratosphere		Troposphere	Stratosphere
a_1	-4.004	-2.68	b_1	-0.1684	-0.276
σ_{a1}	0.0457	0.0592	σ_{b1}	0.00489	0.00582
a_2	0.1729	0.2285	b_2	0.1550	0.2136
σ_{a2}	0.0146	0.0168	σ_{b2}	0.0148	0.0173
a_3	-2.00	-1.473	b_3	-2.072	-1.385
σ_{a3}	0.0225	0.0356	σ_{b3}	0.0236	0.0337
a_4	-0.00054	-0.00295	b_4	-0.00054	-.00307
σ_{a4}	.0000041	.000026	σ_{b4}	.0000036	.0000181

L may be written, for example, for Model (1), in the troposphere as: $L=10^{-4}\dfrac{\left(\sigma_v^2\right)^{.173}}{\left(\omega_B-.00054\right)^2}$, which suggests that L may scale with the variance of the wind speed and inversely with the Brunt-Vaisala frequency. In fact the outerscale of inertial range turbulence L_0 is proportional to $\varepsilon^{\frac{1}{2}}\omega_B^{-\frac{3}{2}}$, where ε is the turbulence dissipation rate and where $\varepsilon^{\frac{1}{2}}$ is proportional to $\sqrt{\overline{v'^2}\,\omega_B^{5}}$, where $\overline{v'^2}$ is the variance of the small scale wind speed fluctuations[12,13], so that

[12] Weinstock, (1978) *Vertical Turbulent Diffusion in a Stably Stratified Fluid*, J. Atm. Sci., V35: 1022.

[13] Hocking, W.K.,(1985) *Measurement of turbulent energy dissipation rates in the middle atmosphere by radar techniques: A review*, Radio Science, 20., (No. 6), 1403-1422.

$L_0 \propto \frac{\sqrt{\overline{v'^2}}}{\omega_B}$. Since the rawinsonde measures large scale wind speed and not $\overline{v'^2}$, Model (1) and Model (2) estimate the microscale through the scaling exponents of σ_v^2 and ω_B.

4. OTHER CASES

4.1. Qualitative Comparison

Figures 1-5 presented in the preceding section was a Pennsylvania State case for Model (1). This section presents additional cases for Pennsylvania State and for other locations and includes cases for both Model (1) and Model (2). Figures 8-11 show the same case as before (L4007) but for Model (2). There exist only minor differences between the C_n^2 results for Model (1) and Model (2) but differences in the magnitude of L are evident. The intended purpose of introducing the average parameters of $\overline{\omega}_B^2$ and $\overline{\sigma}_v^2$ in Model (2) is to provide an adjustment for low winds aloft versus jet stream conditions. Figures 12-19 show another Pennsylvania State University thermosonde flight (L4044). Model (1) is presented in Figures 13-16 while Model (2) is presented in Figures 17-19. This flight differs from L4007 in the very low C_n^2 values in the troposphere from 6-10 km and also in the peak enhancement of C_n^2 just above the tropopause at 13 km. Figure 15 shows that the model tracks the low tropospheric values of C_n^2 as well as the 13 km enhancement. Examination of the Brunt-Vaisala frequency plot and the wind speed variance plot in Figure 15 reveals that the C_n^2 enhancement can be traced to the enhancement of these parameters at 13 km.

Figures 20-28 show a thermosonde flight (L1014) conducted at Champaign, Illinois on the night of 14 June , 1988. Figures 21-24 show the results for Model (1). Figure 25 presents a plot of the shear and Richardson number for comparison to the model. Figures 26-28 show the results for Model (2). Even though the model constants are those that were evaluated for the Pennsylvania State campaign, visual examination will reveal very good agreement between the thermosonde C_n^2 and the model C_n^2. Note particularly the level of agreement between L of the data and L of the model in Figure 22, especially at 7 km. Again this agreement can be traced to enhancements in the Brunt-Vaisala frequency and wind speed variance. Although the Richardson number criterion for turbulence is not invoked in the present model, there does exist a strong feature in the Richardson number plot in Figure 25 at 7 km. This observation suggests that the relationship of local microshear and Brunt-Vaisala frequency can be represented by scaled rawinsonde measurements of Brunt-Vaisala frequency and wind speed variance as depicted in Figure 23.

Figures 29-33 show a thermosonde flight (M0516) conducted at a desert site in New Mexico on the night of 5 September , 1984. Figures 30-32 show the results for Model (1) and Figure 33 shows the C_n^2 result for Model (2). Again the same model constants are used but applied to a climatologically different site. Comparison of Figures 29 with figures 32 and 33 show good agreement. Model (2) shows slight improvement in the stratosphere.

Figures 34-37 show another thermosonde flight (M6385) conducted at the same desert site as M0516 but at a different time of year (3 March 1985). Figures 35-36 show the results for Model (1) and Figure 37 shows the C_n^2 result for Model (2). This case presents a challenge to the model because no winds aloft measurements were available. Lacking the measured wind speeds, the model was calculated for an arbitrary RMS wind speed of 1 m/s. An

examination of the agreement between the thermosonde C_n^2 profile in Figure 34 and the model in Figure 36 suggests that the scaled Brunt-Vaisaia frequency alone may be sufficient to characterize C_n^2 in the absence of very strong shear layers. This concept will be examined further in the next section.

4.2. Quantitative Comparison

A parameter that is sometimes used in describing optical turbulence is the isoplanatic angle. This is an altitude weighted integral of C_n^2 that has significance in optical imaging but which can also serve as a basis of quantitative comparison between measurements of different instruments or between measurement and model. The isoplanatic angle is evaluated as :

$$\Theta_0 = \left[2.95k^2 \int_0^\infty C_n^2(h) h^{-\frac{5}{3}} dh \right]^{-\frac{3}{5}}$$

where h is height above ground and k is wavenumber. For the purposes of this section, the limits of integration are taken over the measured thermosonde altitude region. Tables 2-5 list Θ_0 for the thermosonde measurements and models at various locations.

Table 2. Isoplantic Angle Calculations for the Pennsylvania State University Campaign. Comparison of Measurement to Model

Pennsylvania State University Campaign			
Θ_0 X 10^{-6} rad			
Flight #	Measurement	Model (1)	Model (2)
L4007	6.6	7.9	7.7
L4012	4.7	8.2	7.4
L4014	6.1	6.4	8.5
L4018	8.0	8.3	8.2
L4019	8.5	9.1	8.8
L4029	5.5	7.4	7.3
L4031	6.4	8.4	8.5
L4032	4.9	7.6	7.7

Table 2. (Continued)			
L4033	6.0	8.0	8.2
L4035	4.7	7.8	7.8
L4037	9.0	8.3	8.2
L4042	9.0	7.4	7.4
L4043	5.1	7.7	7.9
L4044	6.9	8.4	8.2
L4045	7.9	8.5	8.2
Average	6.6	8.0	8.0
Std. Dev.	1.5	.61	.44

Table 3 Isoplanatic Angle Calculations for Champaign Illinois Campaign. Comparison of Measurement to Model

Champaign, Illinois Campaign			
Θ_0 X 10^{-6} rad			
Flight #	Measurement	Model (1)	Model (2)
L0553	10.	8.1	8.7
L0554	12.	9.3	9.3
L1006	11.	9.1	8.3
L1014	8.0	8.5	8.6
L3990	6.8	9.9	9.9
Average	9.6	9.0	9.0
Std. Dev.	1.9	.62	.57

Table 4. Isoplanatic Angle Calculations for New Mexico Campaign - Sept 1984. Comparison of Measurement to Model

New Mexico Campaign - Sept. 1984			
$\Theta_0 \times 10^{-6}$ rad			
Flight #	Measurement	Model (1)	Model (2)
M0516	11.	8.0	9.0
M0522	7.5	6.8	6.1
M1880	11.	9.3	10.
M1886	3.5	7.9	8.9
Average	8.2	8.0	8.6
Std. Dev.	3.1	.87	1.5

Table 5. Isoplanatic Angle Calculations for New Mexico Campaign - March 1985. Comparison of Measurement to Model

New Mexico Campaign - March 1985			
$\Theta_0 \times 10^{-6}$ rad			
Flight #	Measurement	Model (1)	Model (2)
M6381	7.2	12.	8.8
M6385	12.	12.	8.7
M6386	6.3	15.	9.0
M6408	5.1	8.9	8.5
M6417	3.9	9.6	8.6
M6563	8.3	11.	10.
Average	7.1	11.	9.0
Std. Dev.	2.5	1.9	2.3

The Pennsylvania State data of Table 2 indicate that, on average, both models overestimate Θ_0 by about 20 percent and reduce the variance of Θ_0 somewhat. Model (1) however provides more variance than Model (2). The Champaign, Illinois data of Table 3 indicate that, on average, both models underestimate Θ_0 by about 6 percent. Model (1) of Table 4 underestimates Θ_0 by 3 percent while Model (2) overestimates by 4 percent. Here, Model (2) provides more variance. The desert site March 1985 data of Table 5 display the most error. Model (1) overestimates Θ_0 by 61 percent while Model (2) overestimates Θ_0 by 27 percent. The problem seems to rest in the fact that no winds aloft data was used for this particular series. In order to apply the model, the RMS wind speed for these flights was arbitrarily set to 1 m/s but the poor result indicates that σ_v^2 should be included after all.

4.3. Comparison with the Dewan et al Model

As described earlier, the Dewan et al. model is a scaled wind shear model. In this section we will examine the Dewan et al. model in terms of the Pennsylvania State University campaign data. Since the model coefficients were derived for 300 m resolution, the applicable rawinsonde parameters of temperature, Brunt-Vaisala frequency, and wind shear were smoothed to 300 m resolution. Figure 38 shows the wind shear profile of flight L4007 that, when applied, results in the model plots of Figures 39-42. Examination of Figures 39 and 40 reveals very little tracking of the small scale profile structure between the thermosonde C_t^2 and model C_t^2 or between the thermosonde smoothed estimate of L and L estimated from the model. Figure 42 also indicates poor tracking of the thermosonde estimate of L and L estimated from the model. On the other hand, examination of Figure 41 reveals that the average profile agrees well with the flight data. Also some of the large scale structure (2-5 km) tracks the thermosonde profile fairly well.

Another flight (L4012) is examined in Figures 43-47. Lack of tracking is again evident in Figures 44, 45, and 47. It would appear that the Brunt-Vaisala term accounts for the large scale tracking of C_n^2 in Figures 41 and 46.

Θ_0 was also calculated for the Dewan et al. model and the results are tabulated in Table 6. On average, the model underestimates Θ_0 by 32 percent. Considering the single parameter estimate of the microscale shear, the model performs well in estimating the C_n^2 average altitude profile, fairly in estimating Θ_0, but poorly in tracking small scale structure in the C_n^2 profile. It appears, therefore, that the microscale shear estimate is insufficient for predicting C_n^2 structure with thicknesses less than 2 km.

Table 6. Isoplanatic Angle Calculations for Dewan et al. Model Comparison of Measurement to Model

$\Theta_0 \times 10^{-6}$ rad		
Flight #	Measurement	Dewan et al. Model
L4007	6.6	4.3
L4012	4.7	2.7
L4014	6.1	.25
L4018	8.0	5.6
L4019	8.5	5.4
L4029	5.5	3.2
L4031	6.4	4.8
L4032	4.9	4.8
L4033	6.0	5.4
L4035	4.7	3.9
L4037	9.0	5.4
L4042	9.0	4.7
L4043	5.1	4.1
L4044	6.9	5.6
L4045	7.9	3.2
		without L4014
Average	6.6	4.5
Std. Dev.	1.5	.97

5. CONCLUSIONS

A comprehensive study of thermosonde data resulted in a simple nighttime quasi-empirical C_n^2 rawinsonde model that takes the form:

$$C_n^2(z) = 2.8[M(z)]^2[L(z)]^{\frac{4}{3}},$$

where

$$M(z) = -79\times10^{-6}\frac{P(z)\omega_B^2(z)}{gT(z)},$$

and where $L(z) = C_1\dfrac{\left(\dfrac{\sigma_v^2(z)}{\overline{\sigma}_v^2}\right)^{C_2}}{\left(\dfrac{\omega_B(z)-C_4}{\overline{\omega}_B}\right)^{C_3}}.$

The model for L(z) is an exponentially scaled estimate of the theoretical description and it uses high resolution rawinsonde data to estimate the altitude dependent parameters σ_v^2 and ω_B^2. The C_n^2 model is independent of location but applicable to a variety a different climatological conditions. Compared to other models, the thermosonde model is either much less complex or shows better fidelity to thermosonde derived measurements.

Thermosondes are reliable instruments for obtaining tropospheric and stratospheric optical turbulence data. When optical turbulence is important in characterizing new sites for vertical paths, the described model may be employed to estimate C_n^2. Many low cost, high resolution rawinsondes can be deployed rapidly to construct a turbulence climatology. Where high resolution data already exists, the proposed model offers significant time, robustness, and cost advantages in exchange for a small computational burden.

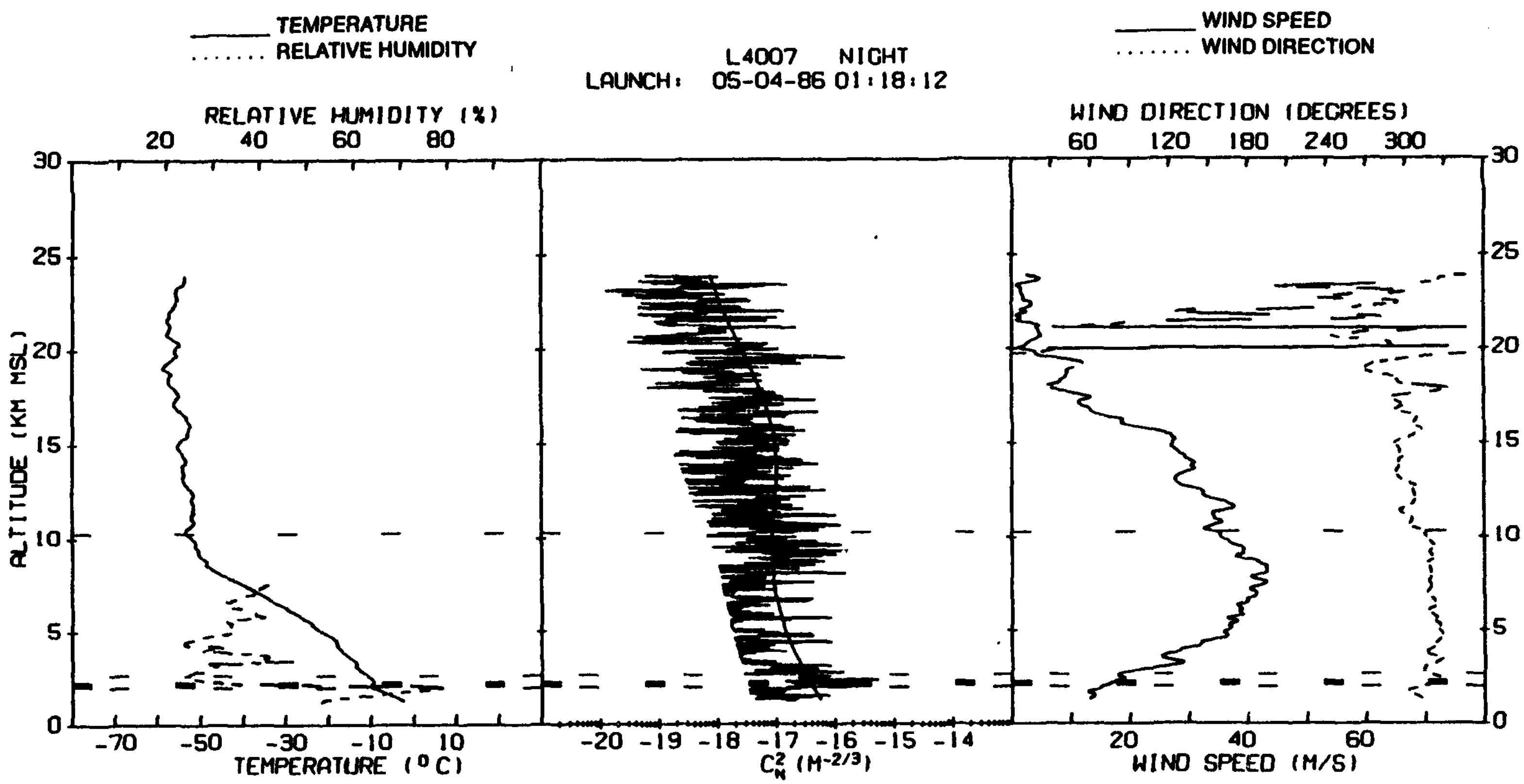

Figure 1. Thermosonde Profiles Measured at Pennsylvania State University, Flight L4007, 4 May, 1986, Temperature, Relative Humidity, C_n^2, Wind Speed, Wind Direction

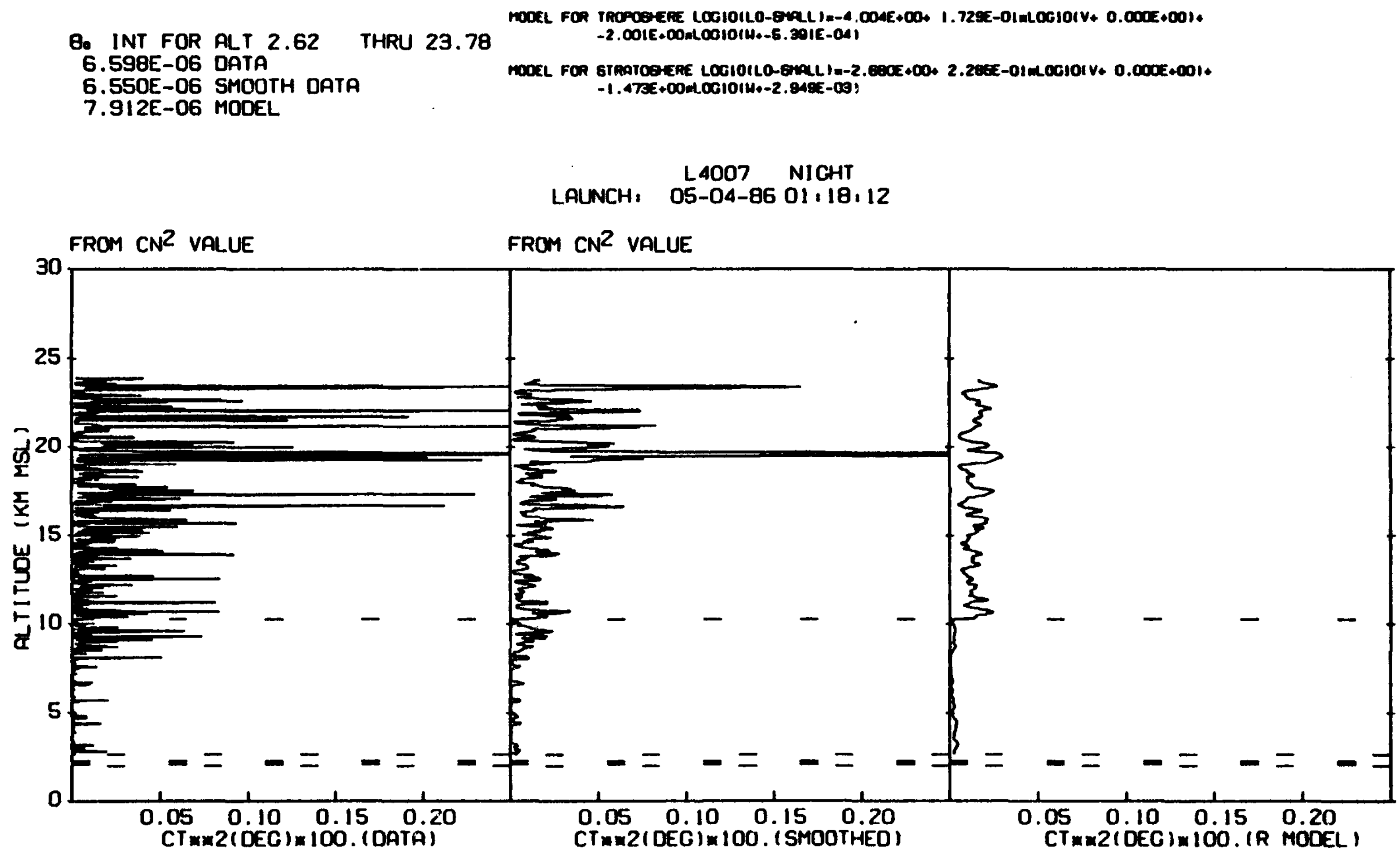

Figure 2. Thermosonde C_t^2 Measurement (Raw and Smoothed) Profiles Compared to Model (1) C_t^2 Profile. Flight L4007

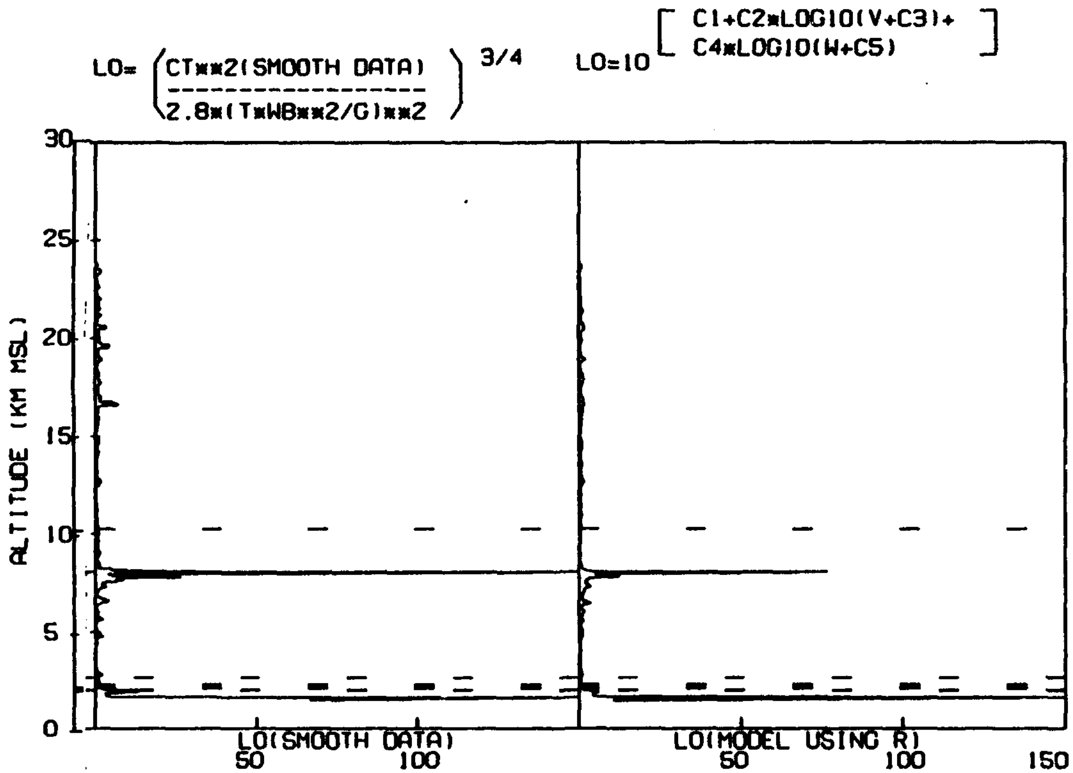

Figure 3. L(z) From Smoothed Data Compared to Model (1). Flight L4007

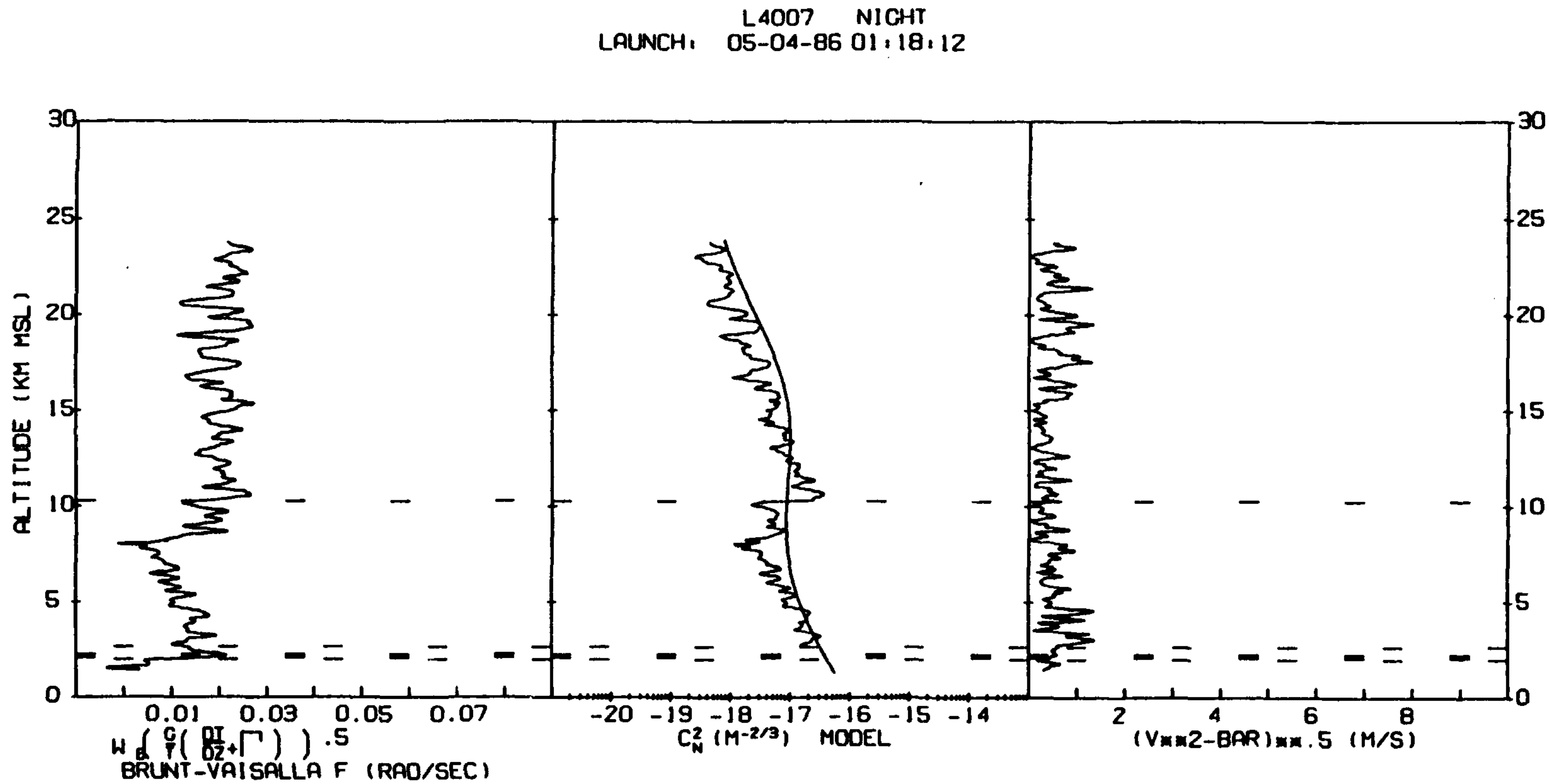

Figure 4. Brunt-Vaisala Frequency and RMS Wind Speed Profiles Derived From Measurement Compared With C_n^2 Profile from Model (1). Flight L4007

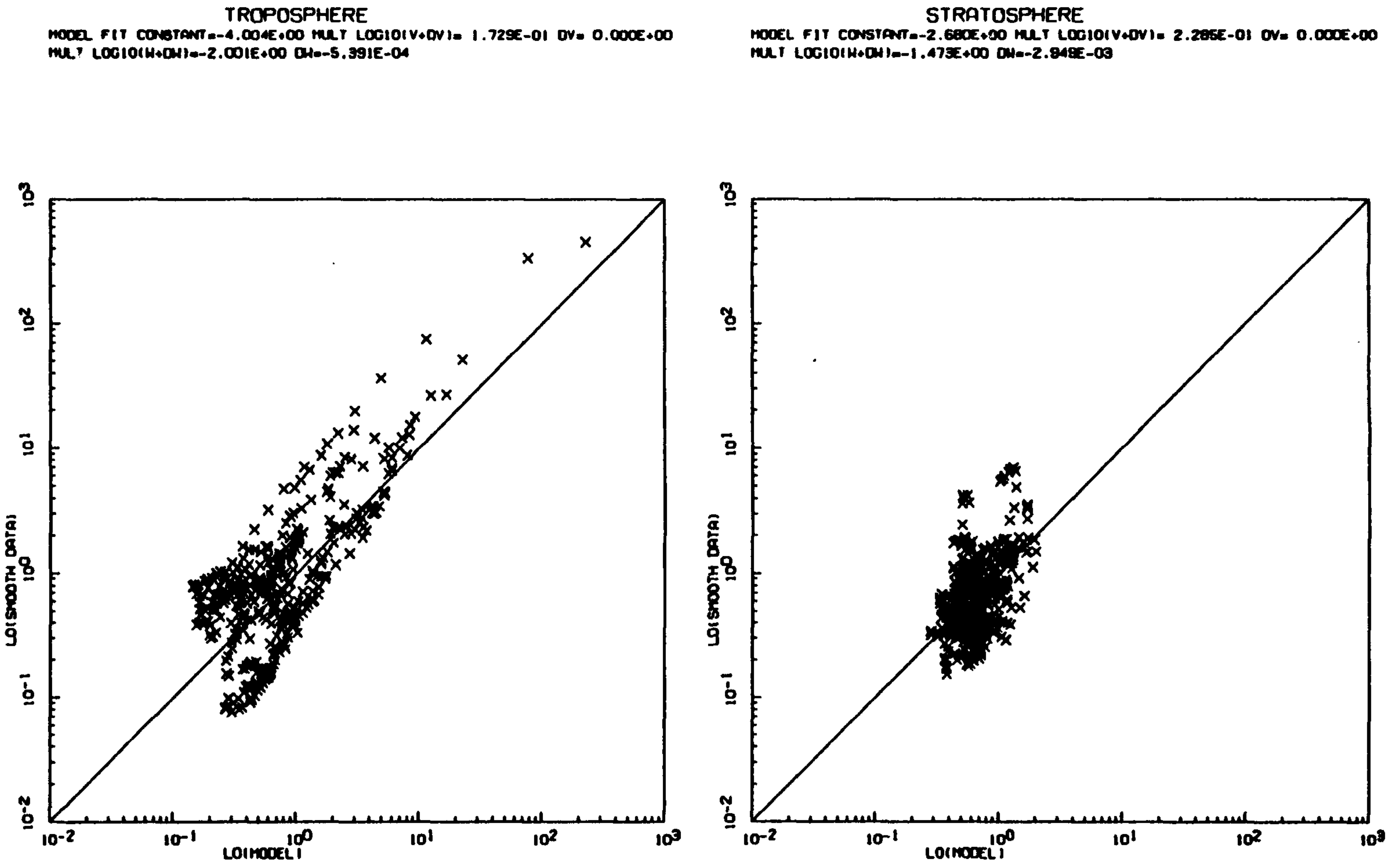

Figure 5. Scatter plot of "L" for Smoothed Thermosonde Measurements Compared With "L" From Model (1). Flight L4007. Leftmost plot for troposphere. Rightmost plot for stratosphere

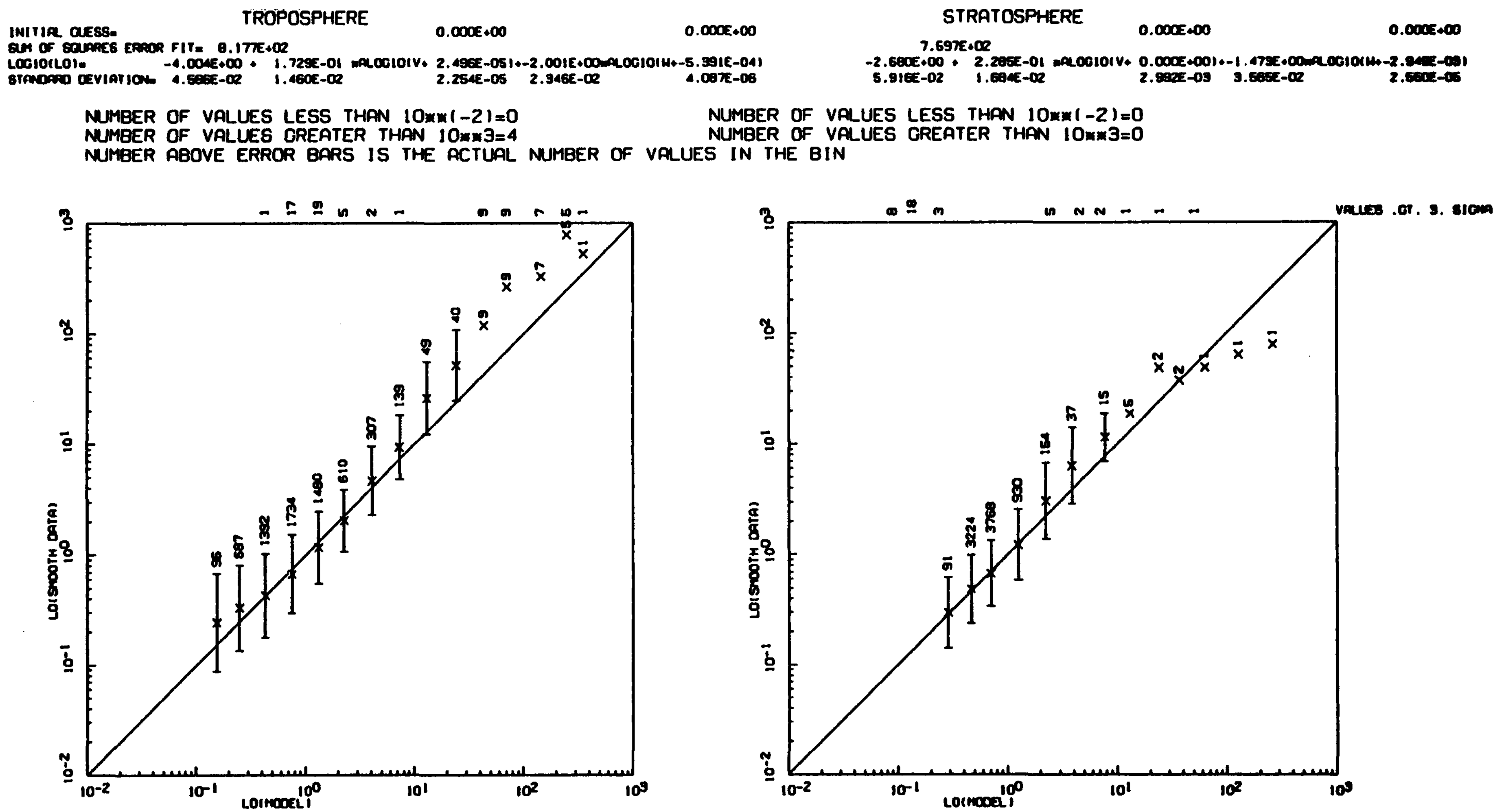

Figure 6. Binned Scatter Plot of Data from Entire Pennsylvania State University Campaign. "L" for smoothed thermosonde measurements compared with "L" from Model (1). A 45 degree slope represents perfect agreement. Error bars represent the standard deviation of the data in each bin. Numbers above the plots are the number of points falling outside three standard deviations. Left-hand plot is troposphere. Right-hand plot is stratosphere

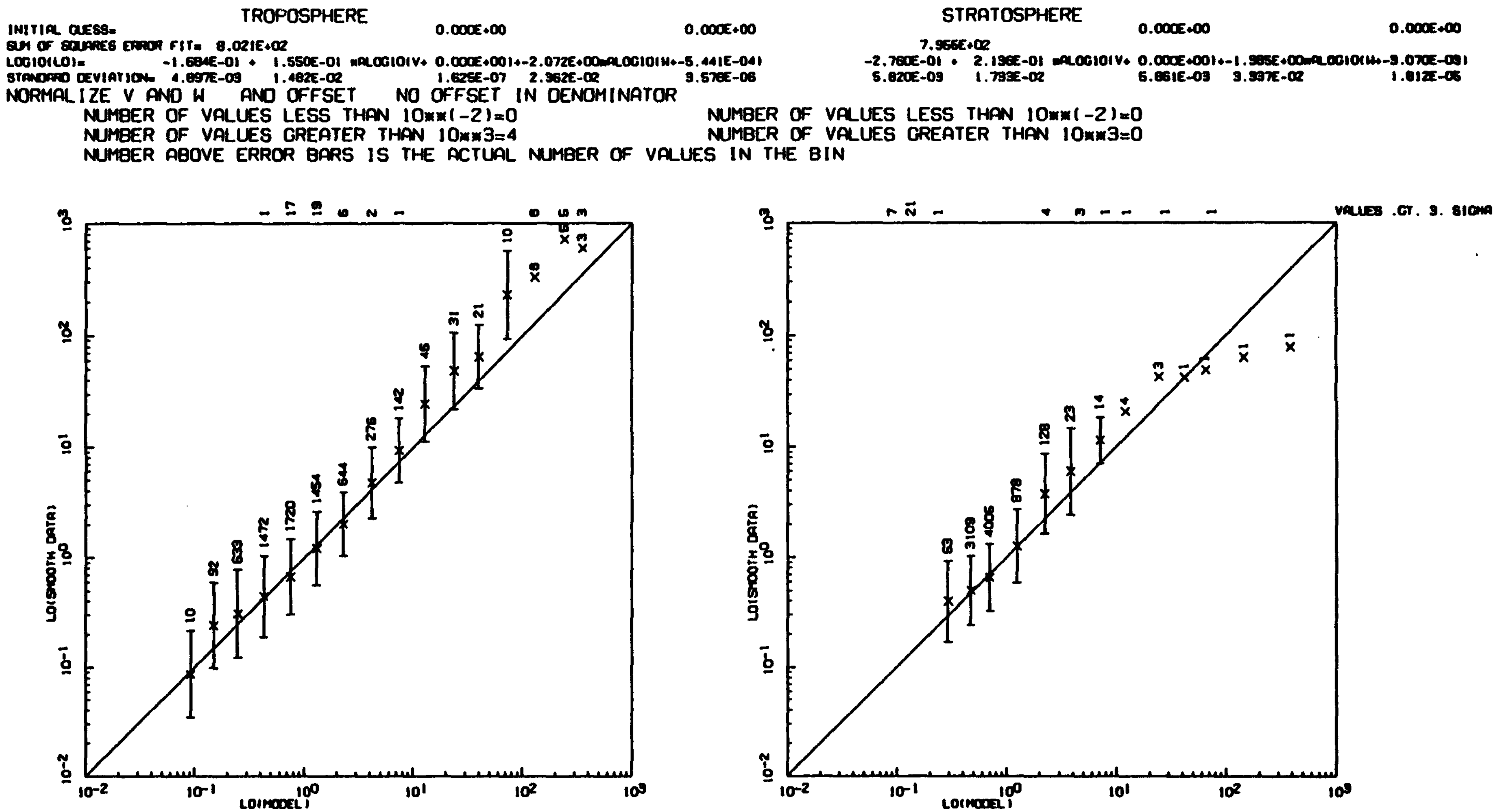

Figure 7. Binned Scatter Plot of Data From Entire Pennsylvania State University Campaign. "L" for smoothed thermosonde measurements compared with "L" from Model (2). A 45 degree slope represents perfect agreement. Error bars represent the standard deviation of the data in each bin. Numbers above the plots are the number of points falling outside three standard deviations. Left-hand plot is troposphere. Right-hand plot is stratosphere

8. INT FOR ALT 2.62 THRU 23.78
6.598E-06 DATA
6.550E-06 SMOOTH DATA
7.674E-06 MODEL

MODEL FOR TROPOSHERE LOG10(L0-SMALL)=-1.684E-01+ 1.550E-01*LOG10((V+ 0.000E+00)/ 5.219E-01)+
-2.072E+00*LOG10((W+-6.441E-04/ 1.264E-02)

MODEL FOR STRATOSHERE LOG10(L0-SMALL)=-2.760E-01+ 2.136E-01*LOG10((V+ 0.000E+00)/ 4.448E-01)+
-1.365E+00*LOG10((W+-3.070E-03) 2.063E-02)

L4007 NIGHT
LAUNCH: 05-04-86 01:18:12

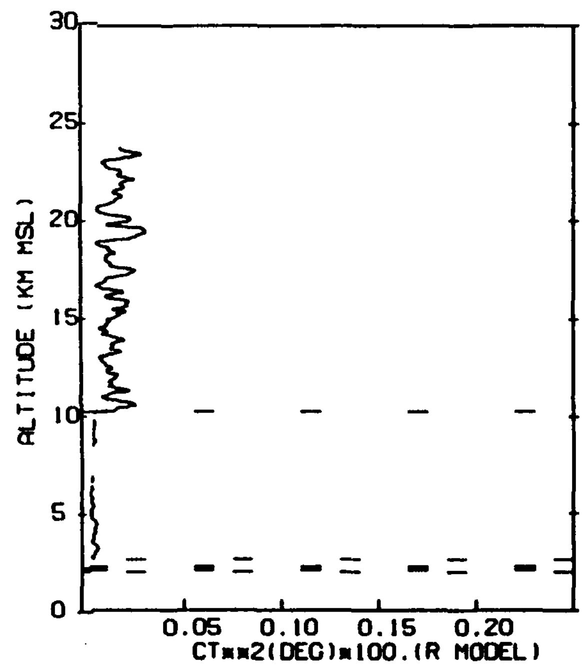

Figure 8. Model (2) C_t^2 Profile. Flight L4007

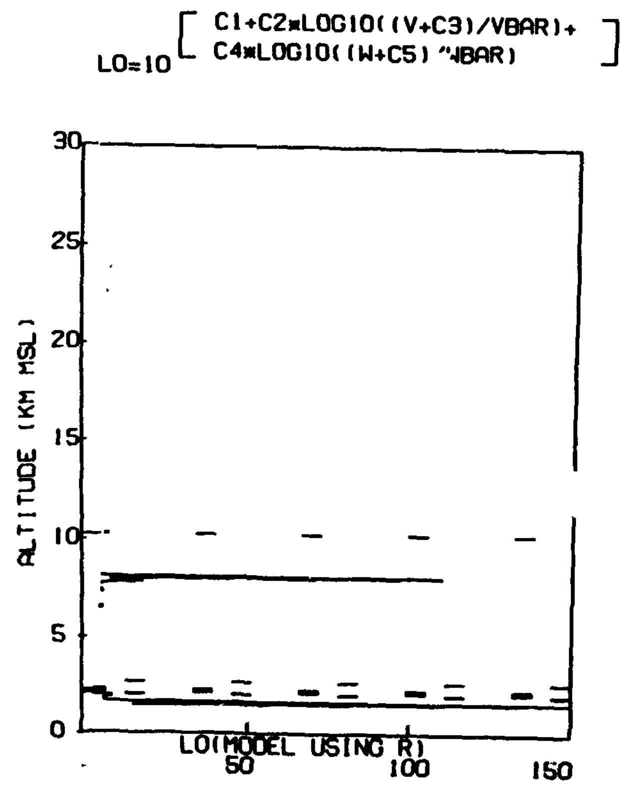

Figure 9. Model (2) "L" Profile. Flight L4007

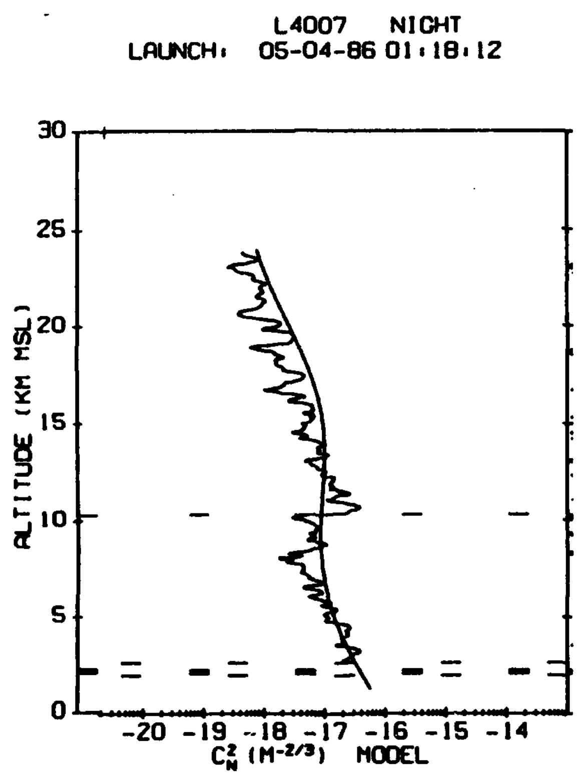

Figure 10. Model (2) C_n^2 Profile. Flight L4007

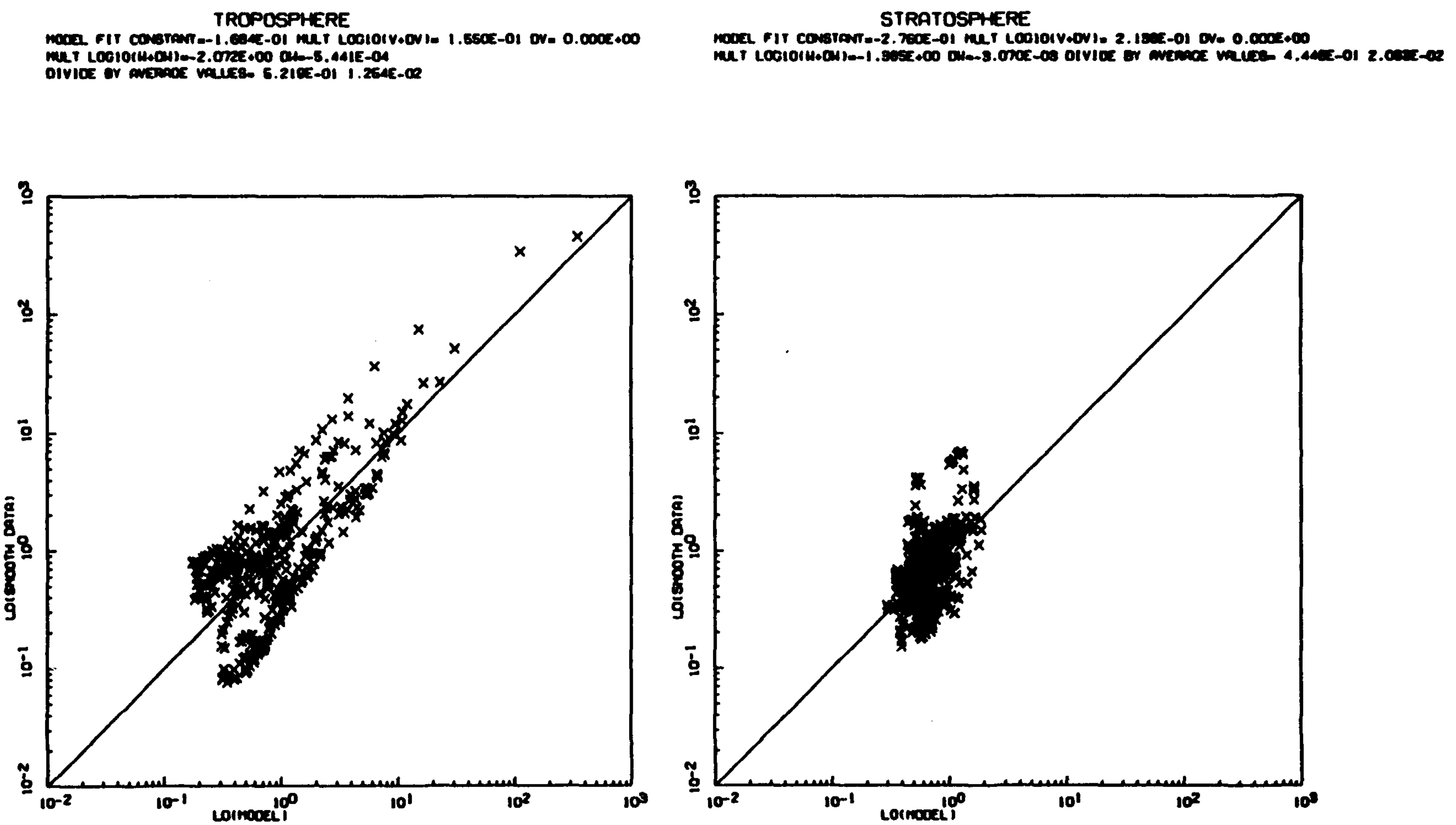

Figure 11. Scatter Plot of "L" For Smoothed Thermosonde Measurements Compared with "L" From Model (2). Flight I4007. Leftmost plot for troposphere. Rightmost plot for stratosphere

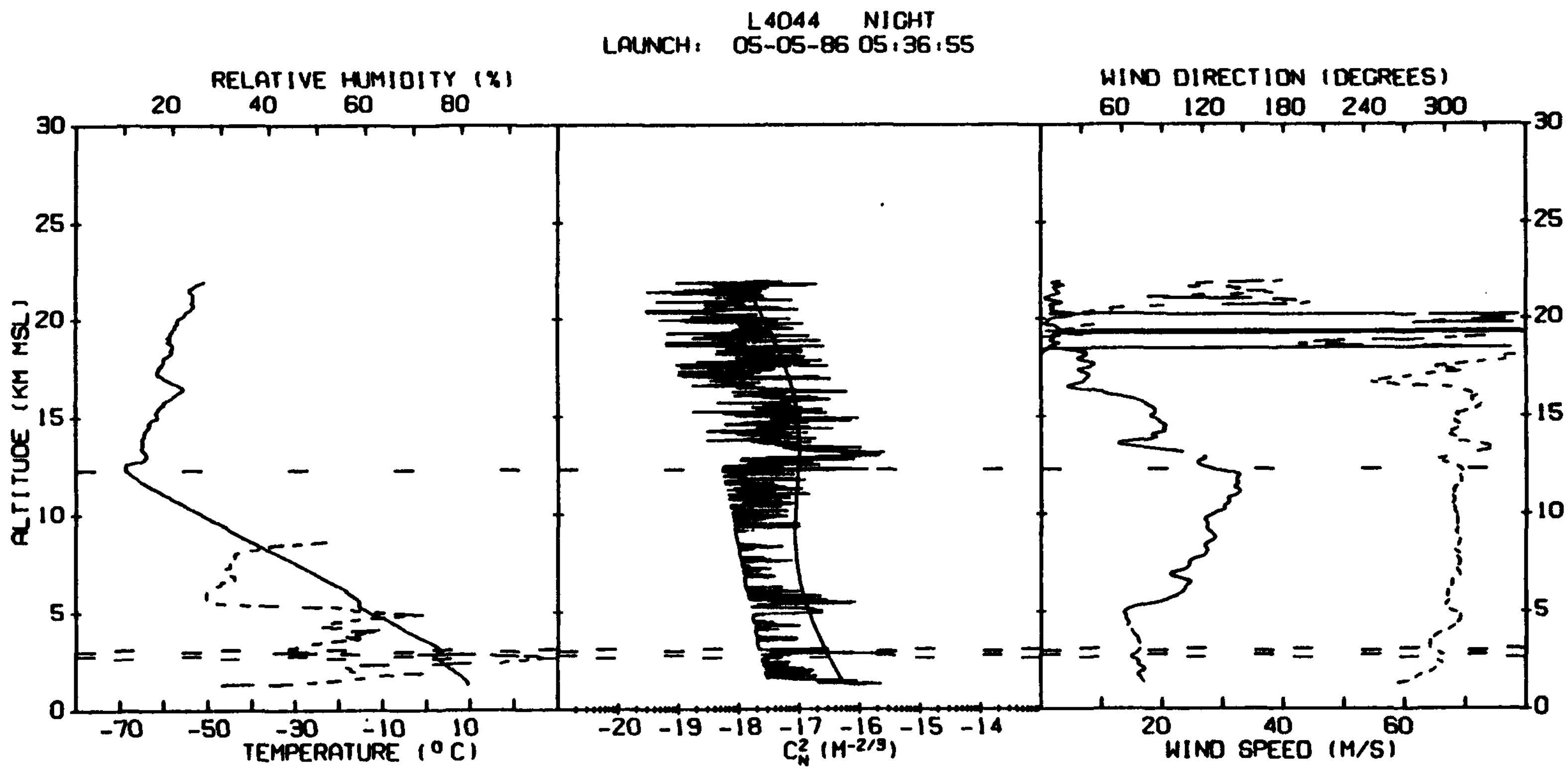

Figure 12. Same as Figure 1 but for Pennsylvania State University Flight L4044

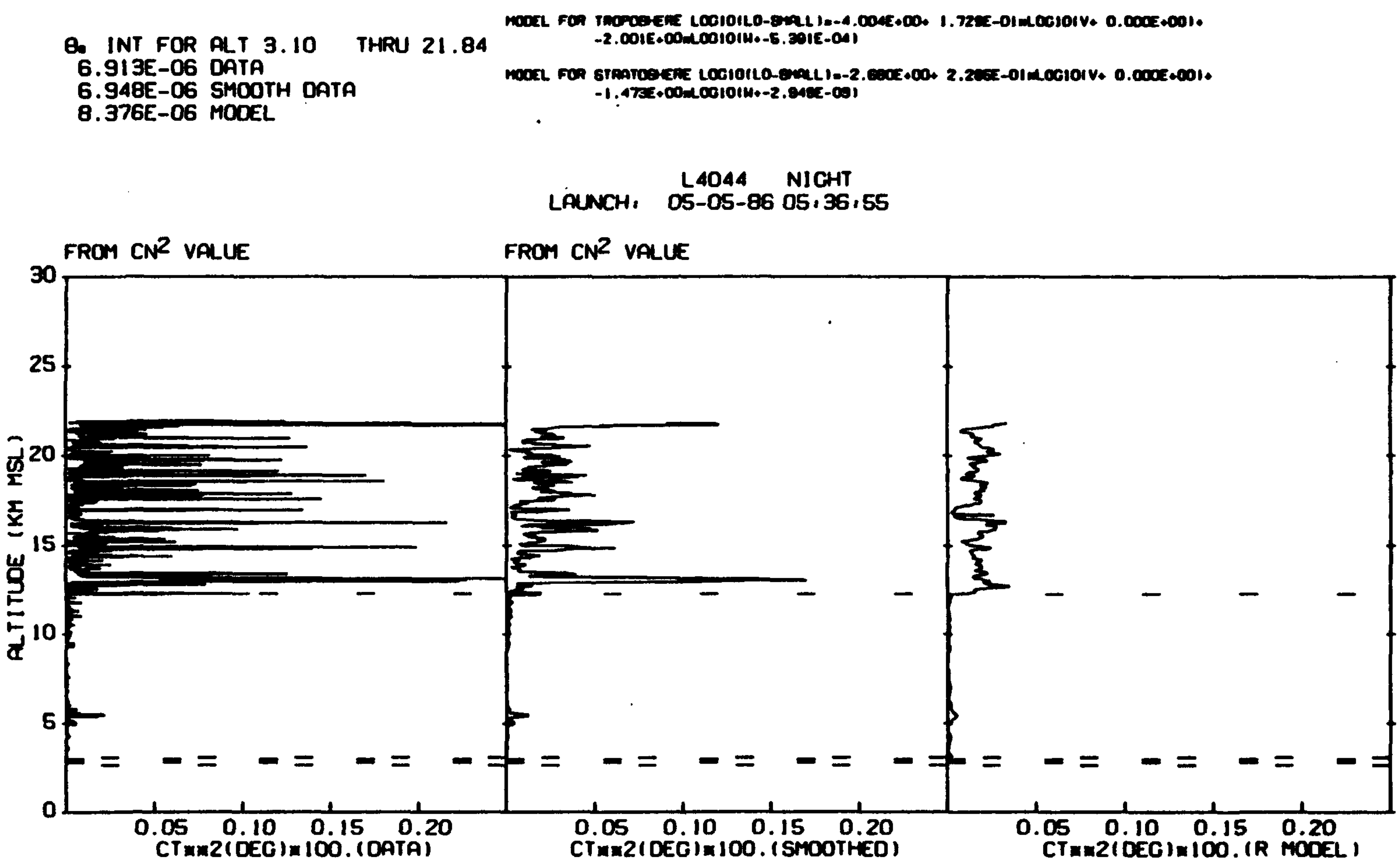

Figure 13. Same as Figure 2 but for Pennsylvania State University Flight L4044

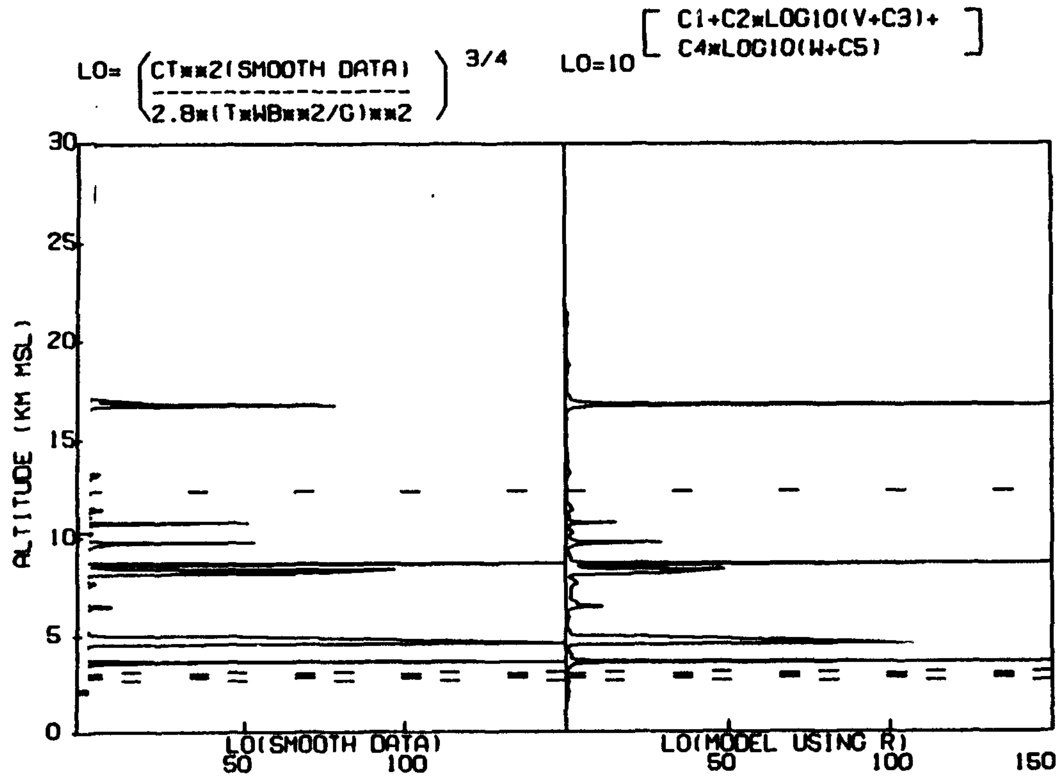

Figure 14. Same as Figure 3 but for Pennsylvania State University Flight L4044

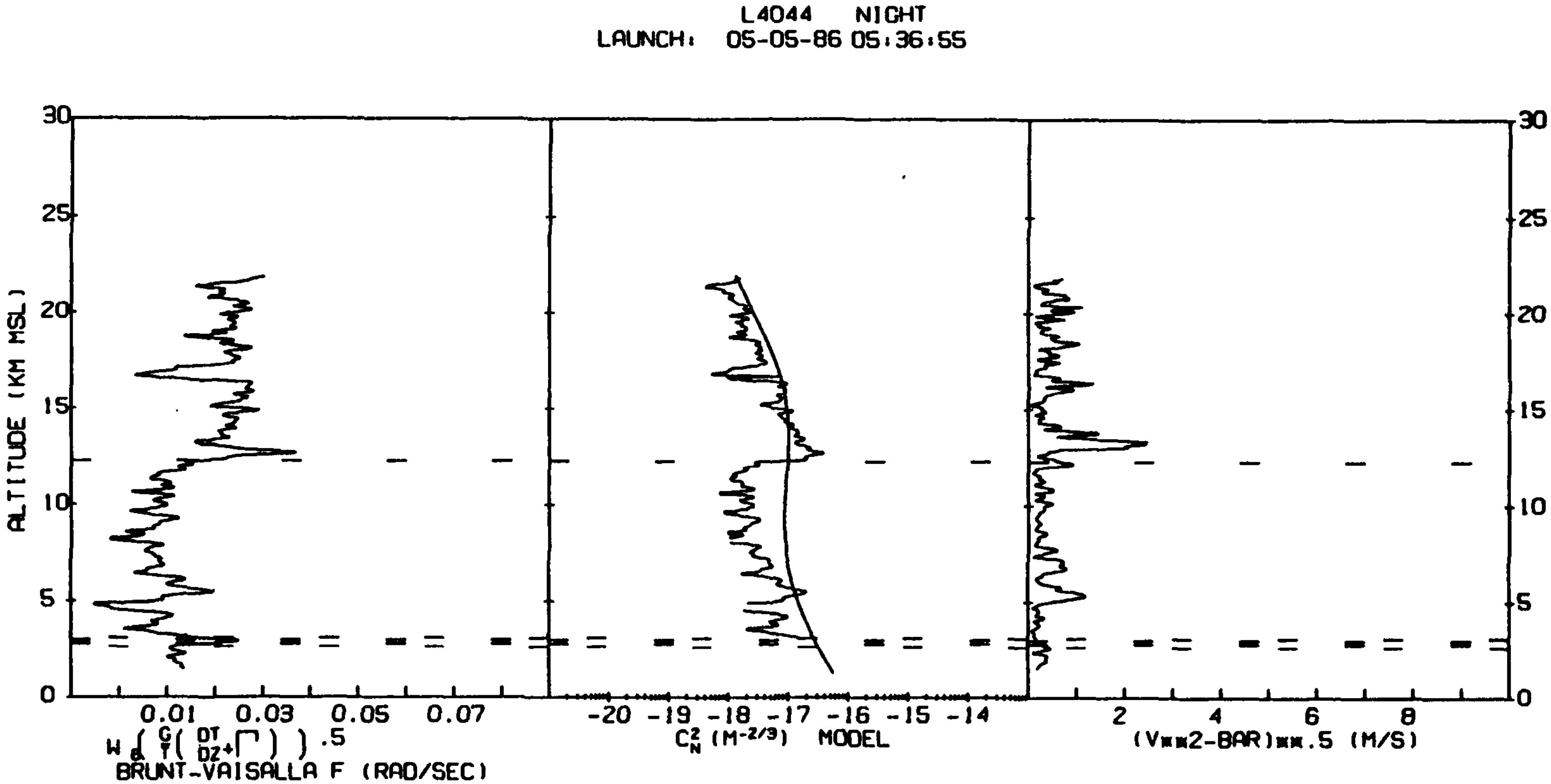

Figure 15. Same as Figure 4 but for Pennsylvania State University Flight L4044

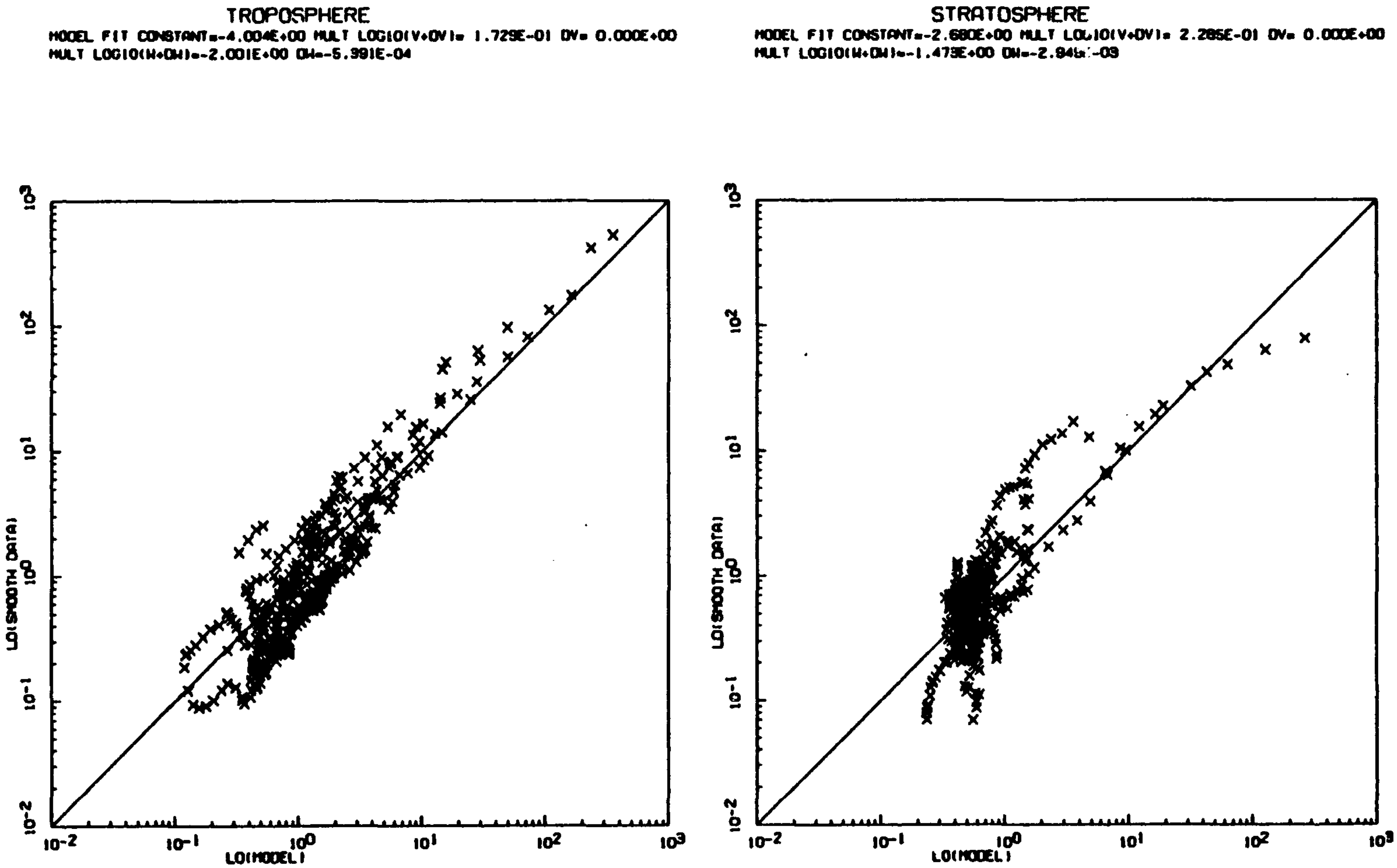

Figure 16. Same as Figure 5 but for Pennsylvania State University Flight L4044

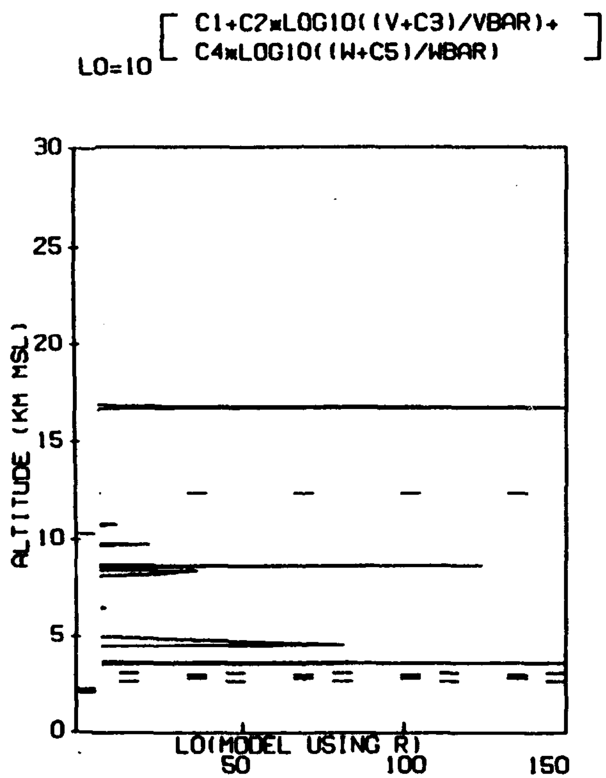

Figure 17. Same as Figure 9 but for Pennsylvania State University Flight L4044

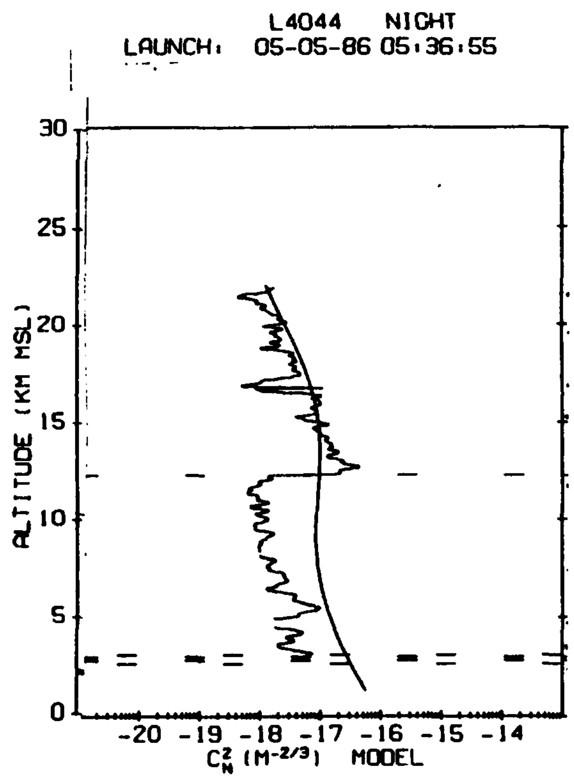

Figure 18. Same as Figure 10 but for Pennsylvania State University Flight L4044

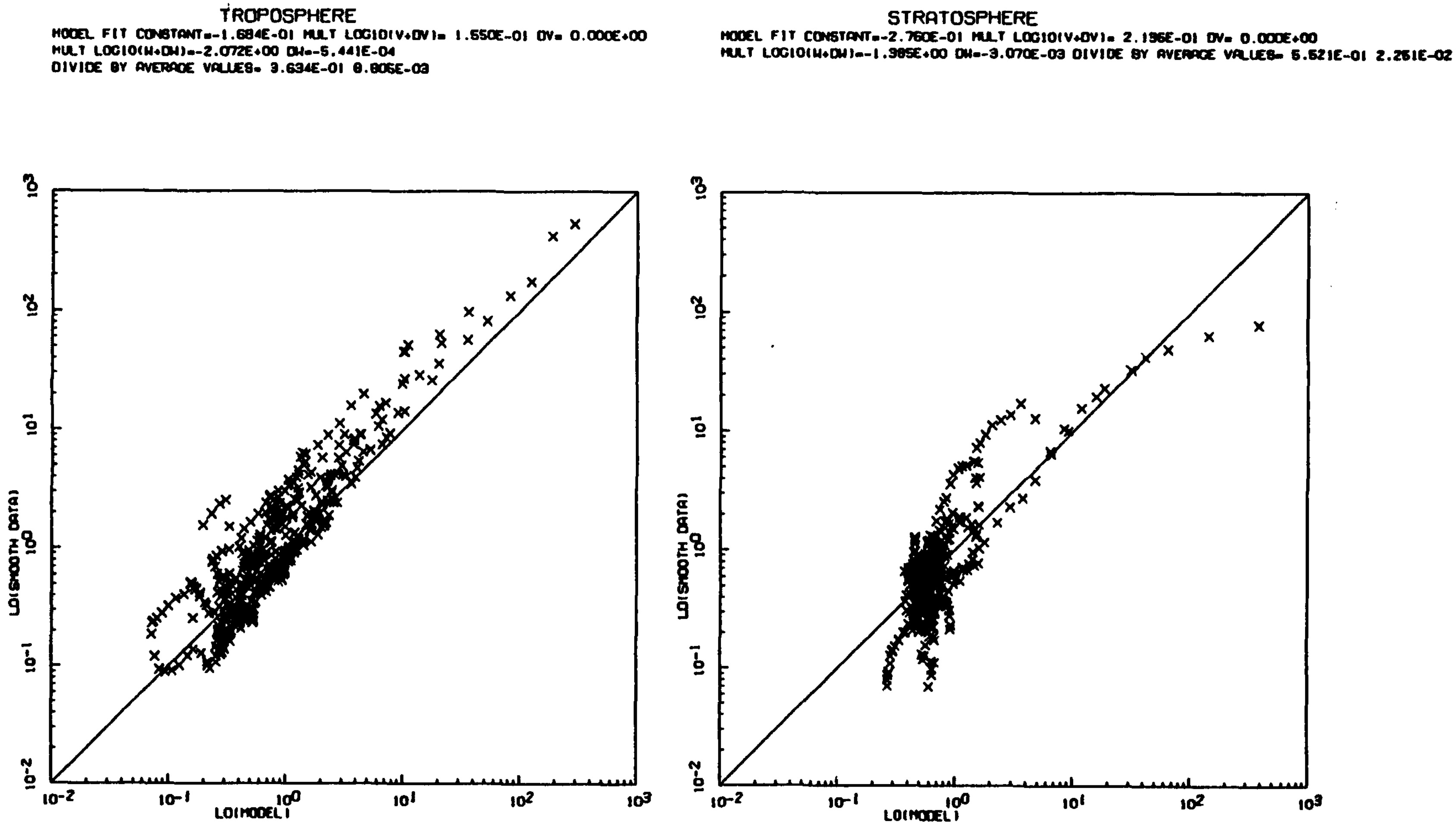

Figure 19. Same as Figure 11 but for Pennsylvania State University Flight L4044

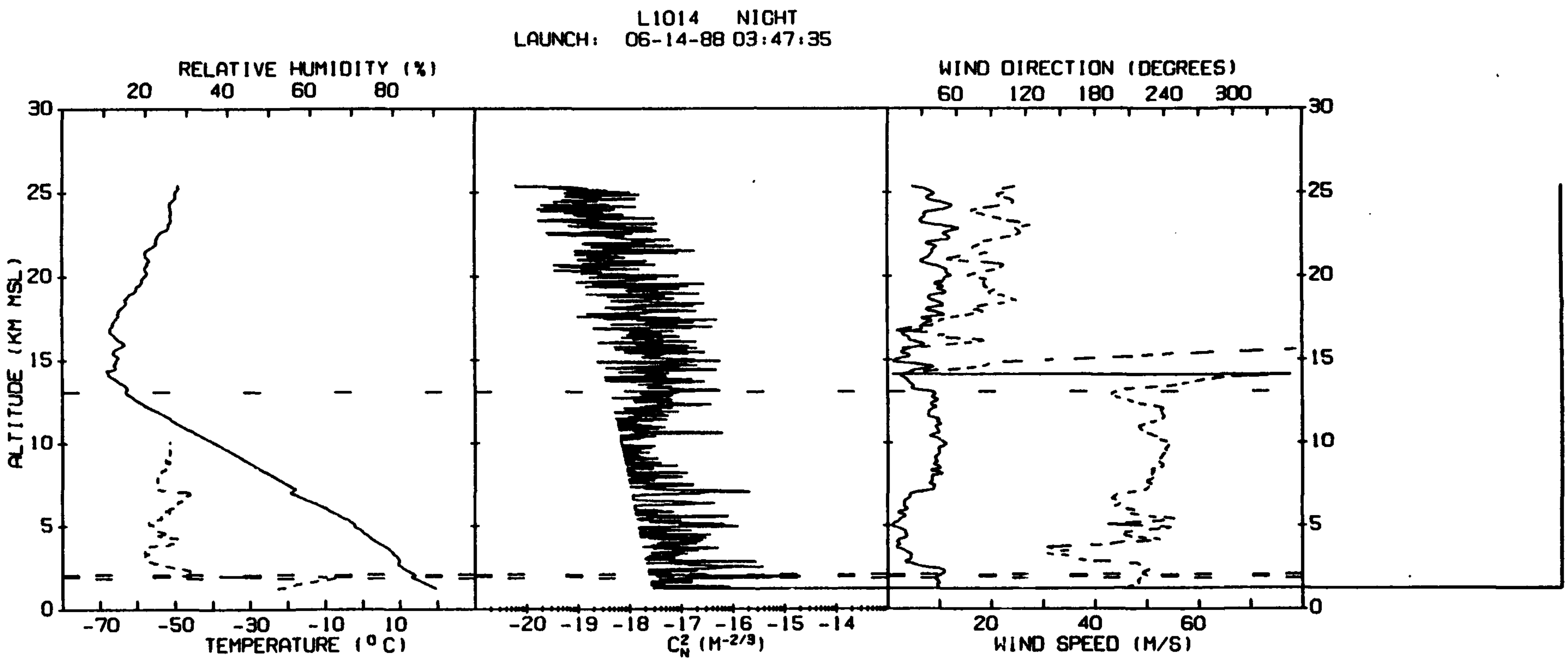

Figure 20. Same as Figure 1 but for Champaign, Illinois Flight L1014, June 1988

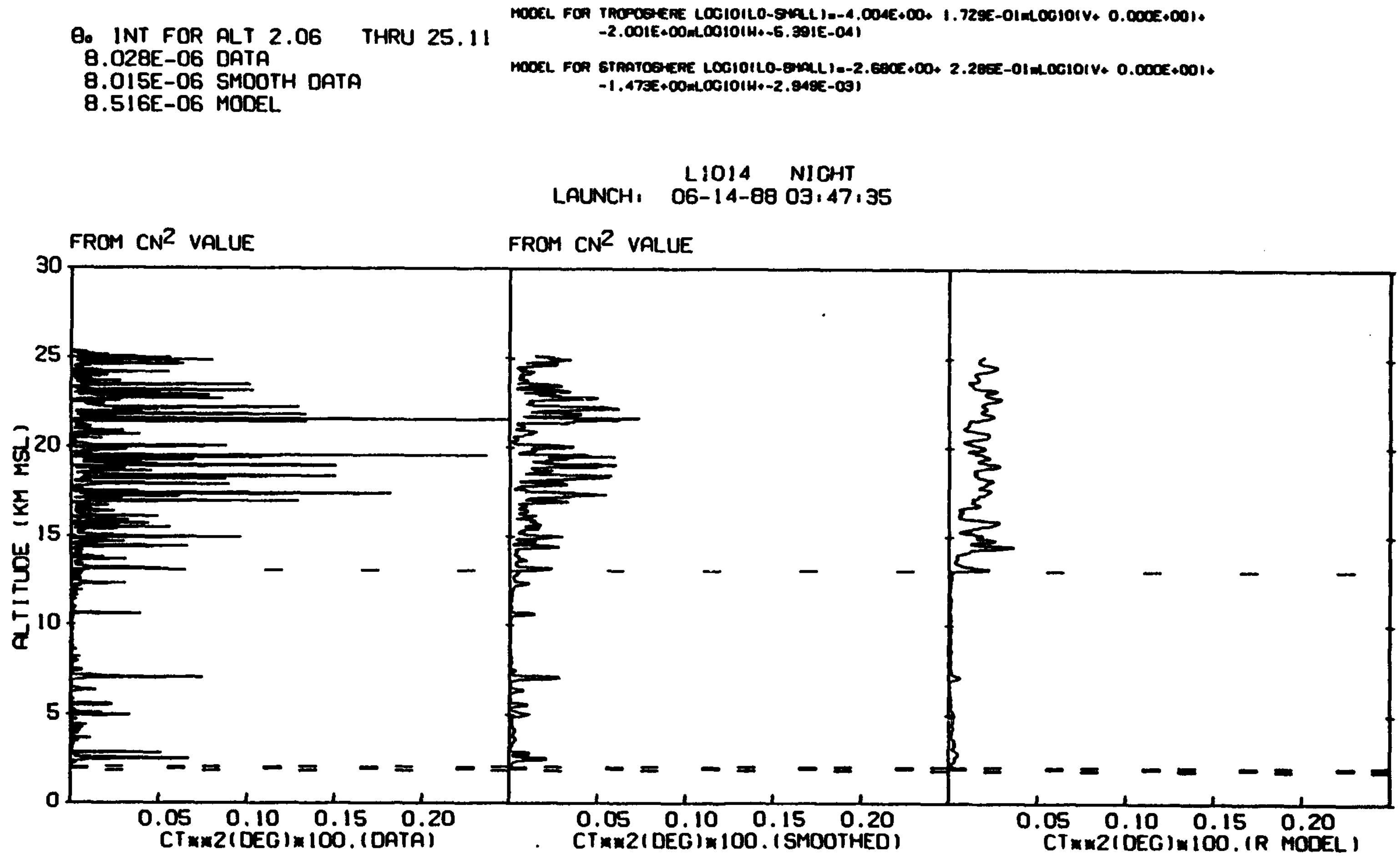

Figure 21. Same as Figure 2 but for Champaign, Illinois Flight L1014, June 1988

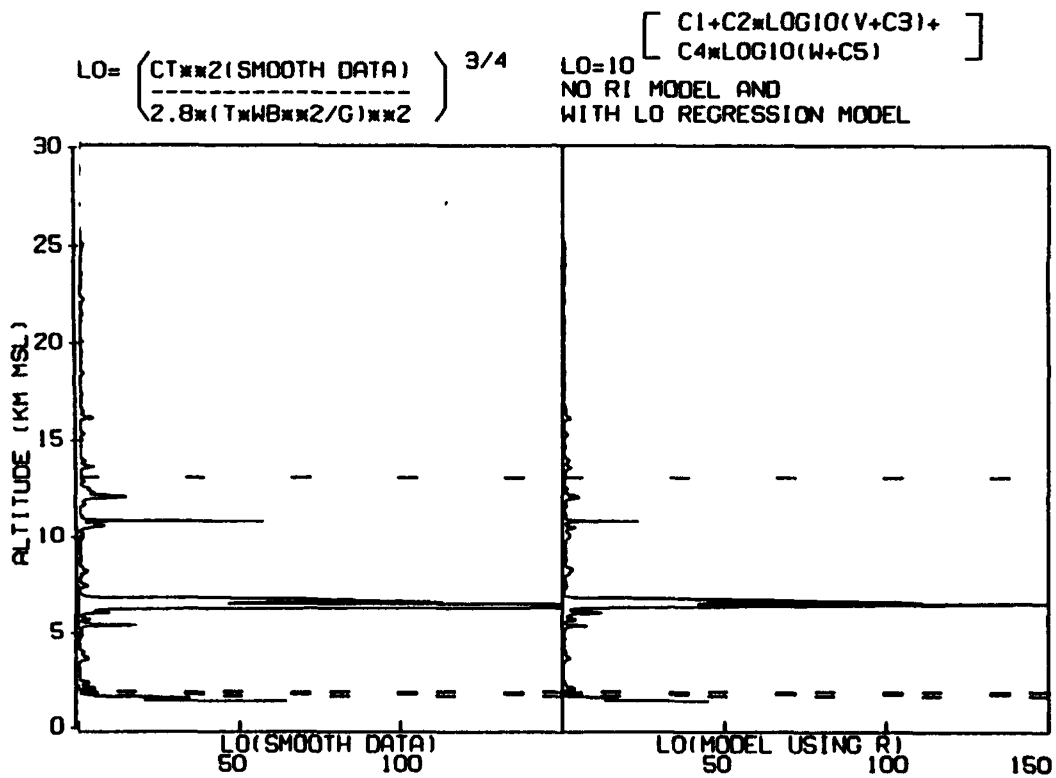

Figure 22. Same as Figure 3 but for Champaign, Illinois Flight L1014, June 1988

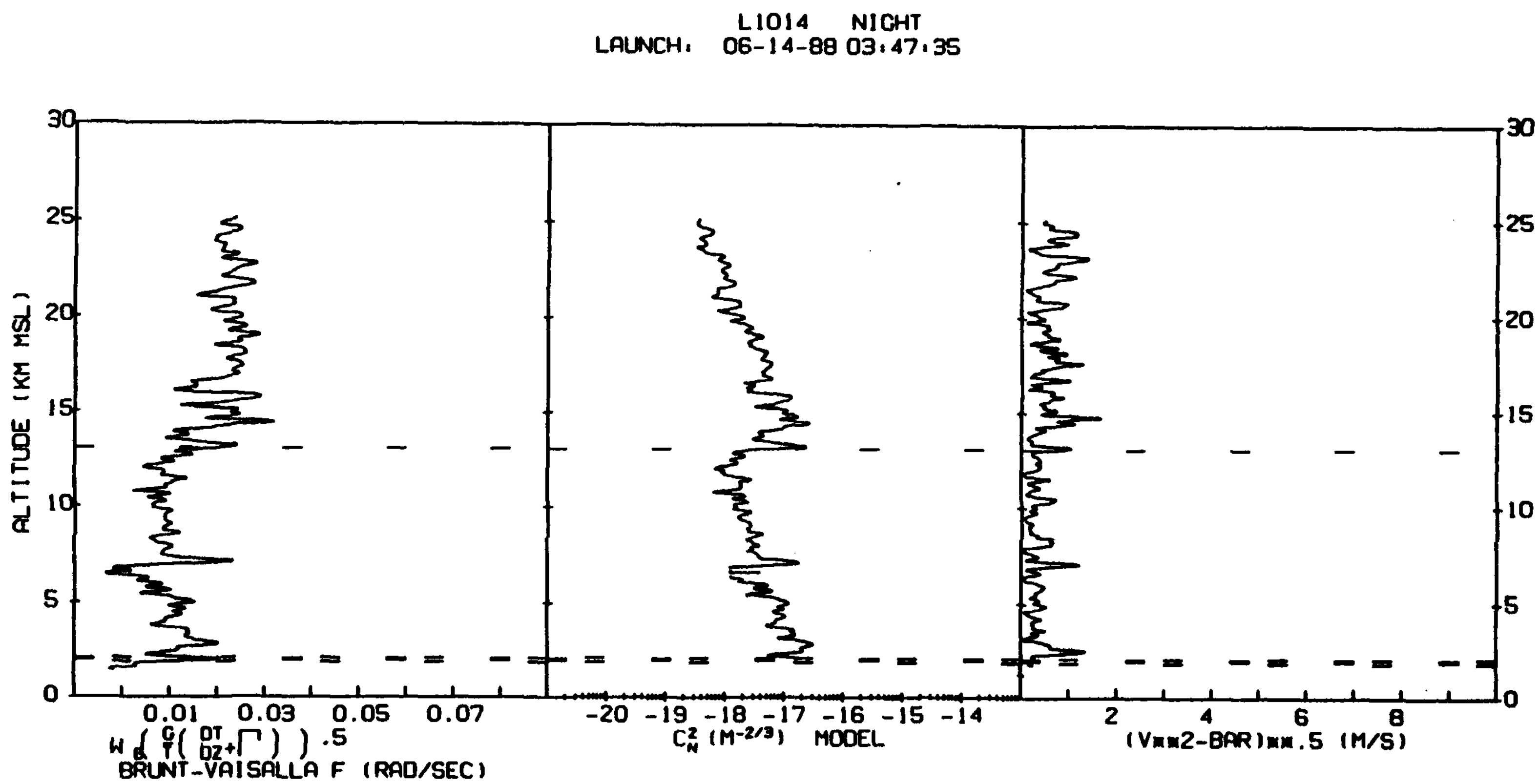

Figure 23. Same as Figure 4 but for Champaign, Illinois Flight L1014, June 1988

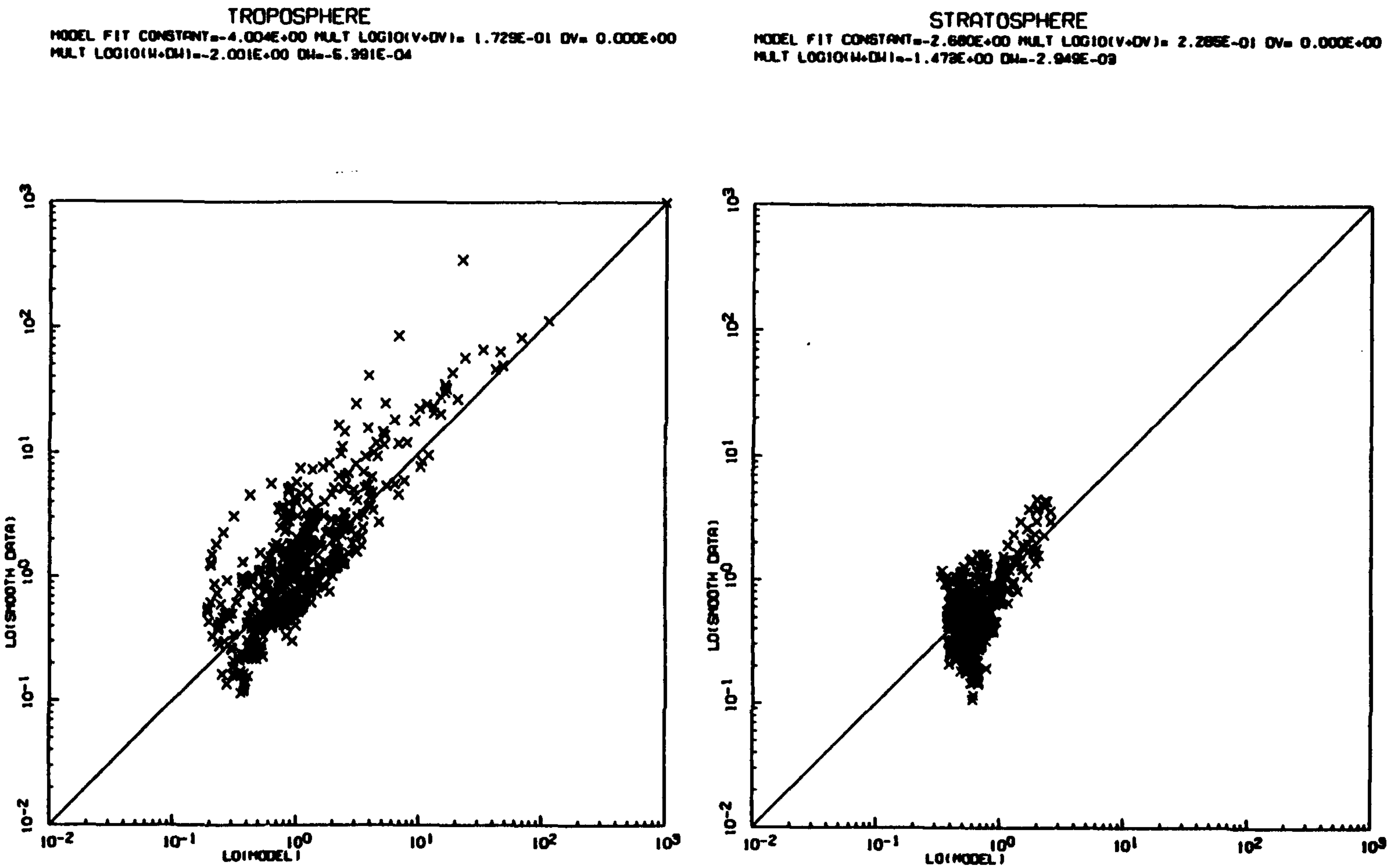

Figure 24. Same as Figure 5 but for Champaign, Illinois Flight L1014, June 1988

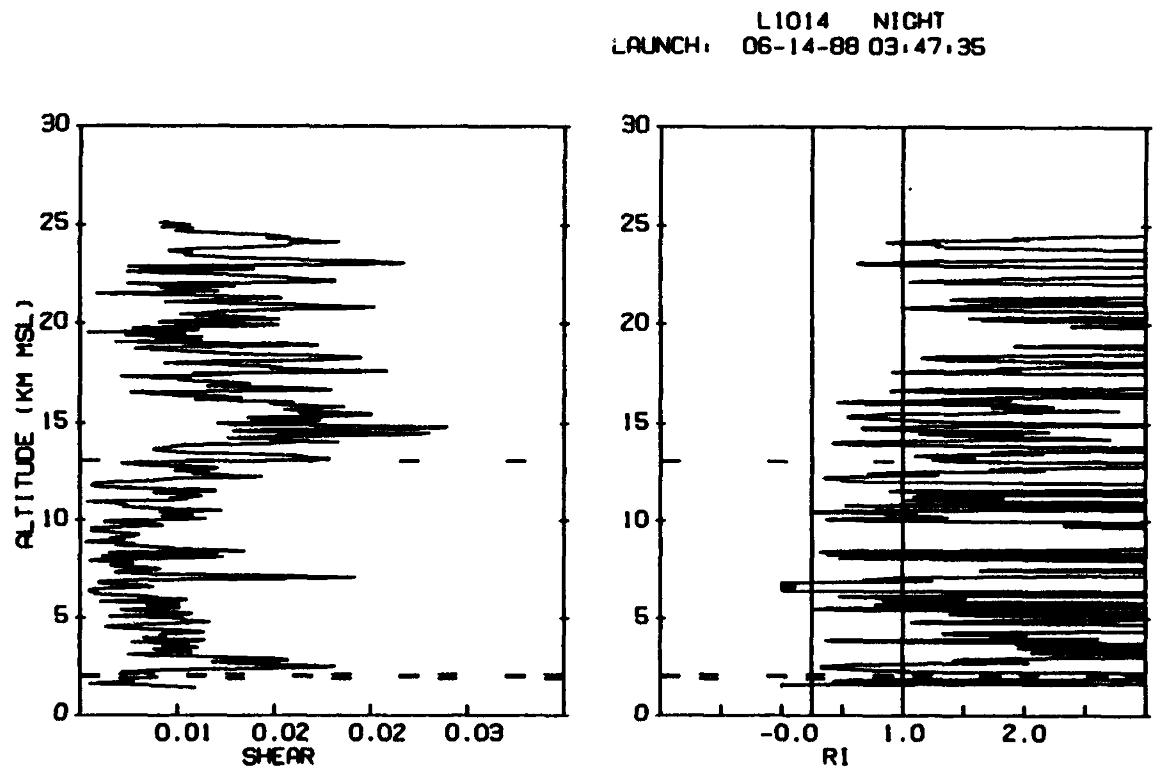

Figure 25. Shear and Richardson Number Profiles Calculated for Champaign, Illinois Flight L1014, June 1988

θ₀ INT FOR ALT 2.06 THRU 25.11
8.028E-06 DATA
8.015E-06 SMOOTH DATA
8.579E-06 MODEL

MODEL FOR TROPOSHERE LOG10(LO-SMALL)=-1.684E-01+ 1.550E-01*LOG10((V+ 0.000E+00)/ 3.391E-01)+
-2.072E+00*LOG10((H+-6.441E-04/ 9.840E-03)

MODEL FOR STRATOSHERE LOG10(LO-SMALL)=-2.760E-01+ 2.136E-01*LOG10((V+ 0.000E+00)/ 5.916E-01)+
-1.385E+00*LOG10((H+-3.070E-03) 2.191E-02)

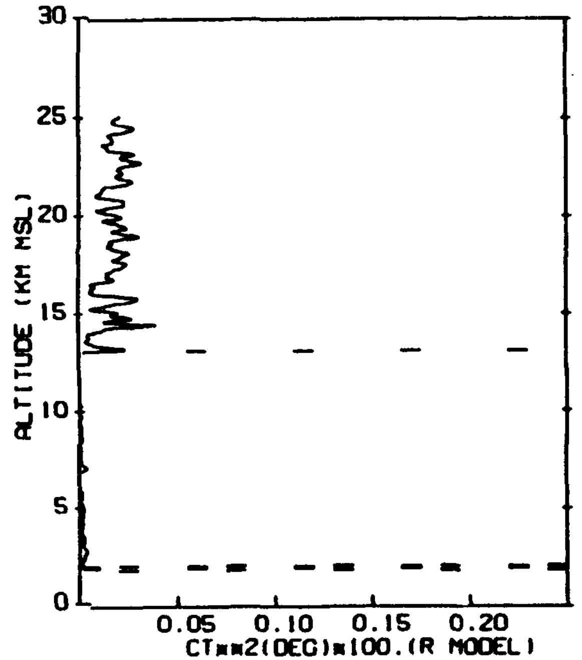

Figure 26. Same as Figure 8 but for Champaign, Illinois Flight L1014, June 1988

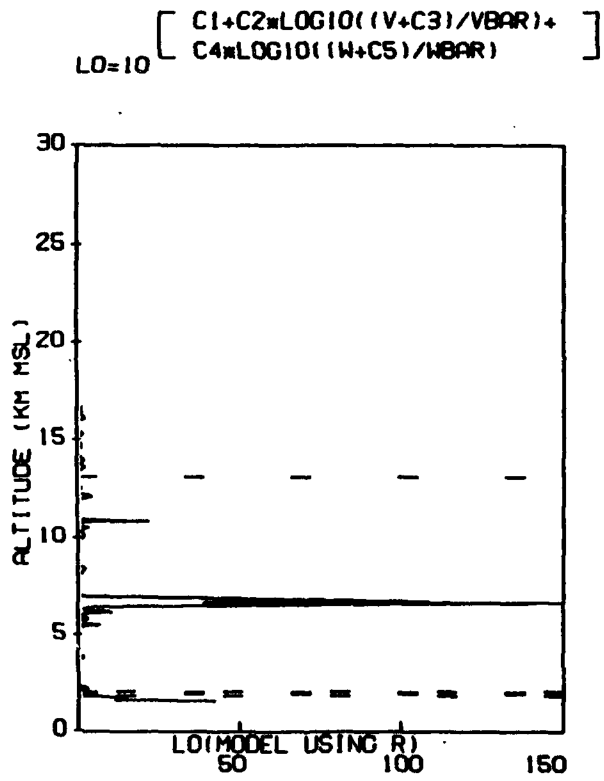

Figure 27. Same as Figure 9 but for Champaign, Illinois Flight L1014, June 1988

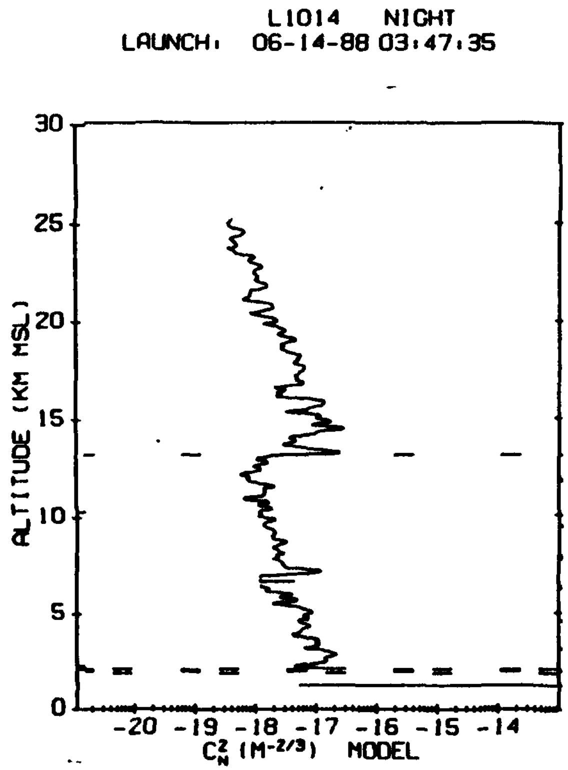

Figure 28. Same as Figure 10 but for Champaign, Illinois Flight L1014, June 1988

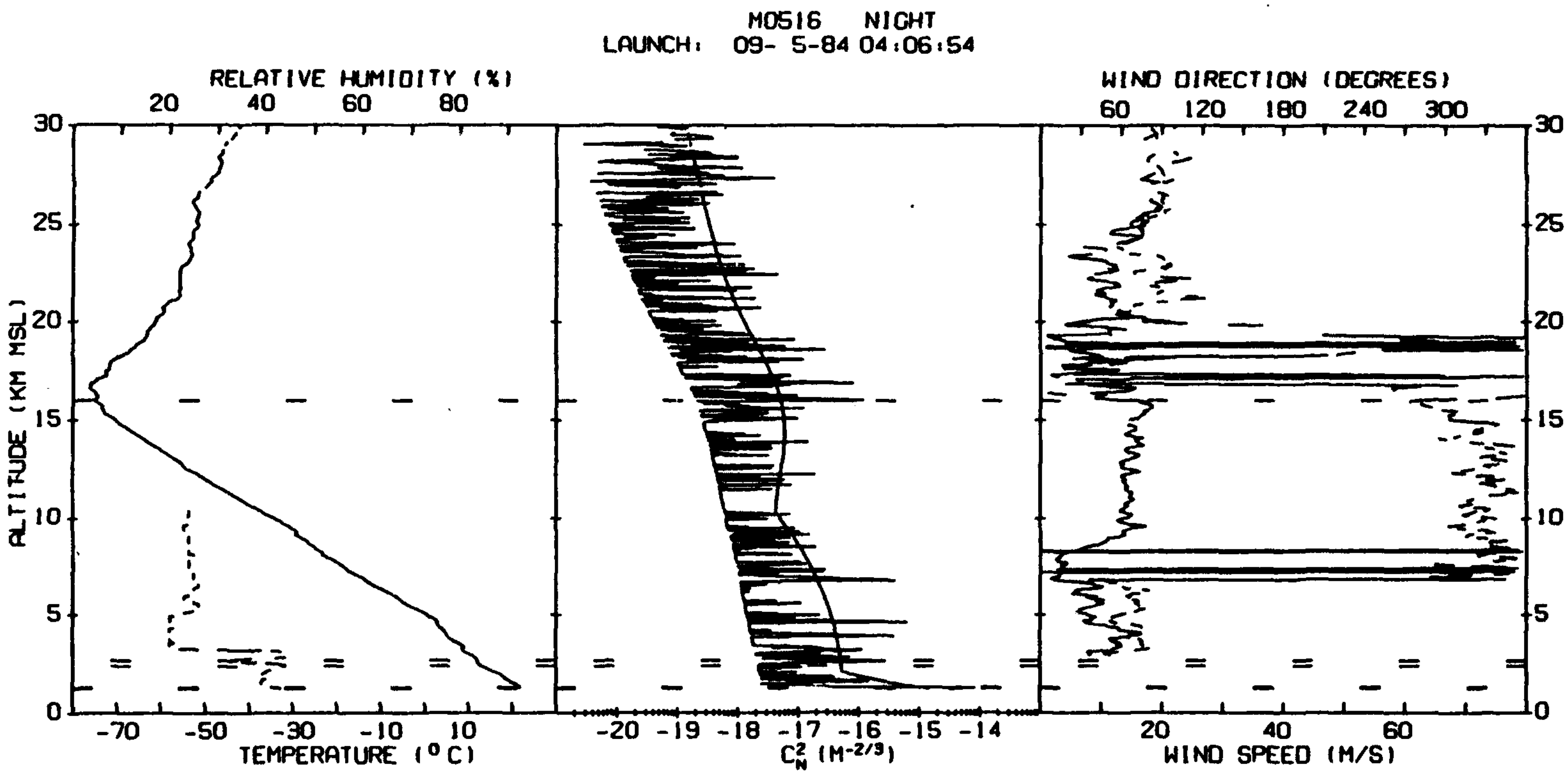

Figure 29. Same as Figure 1 but for New Mexico Flight M0516, September 1984

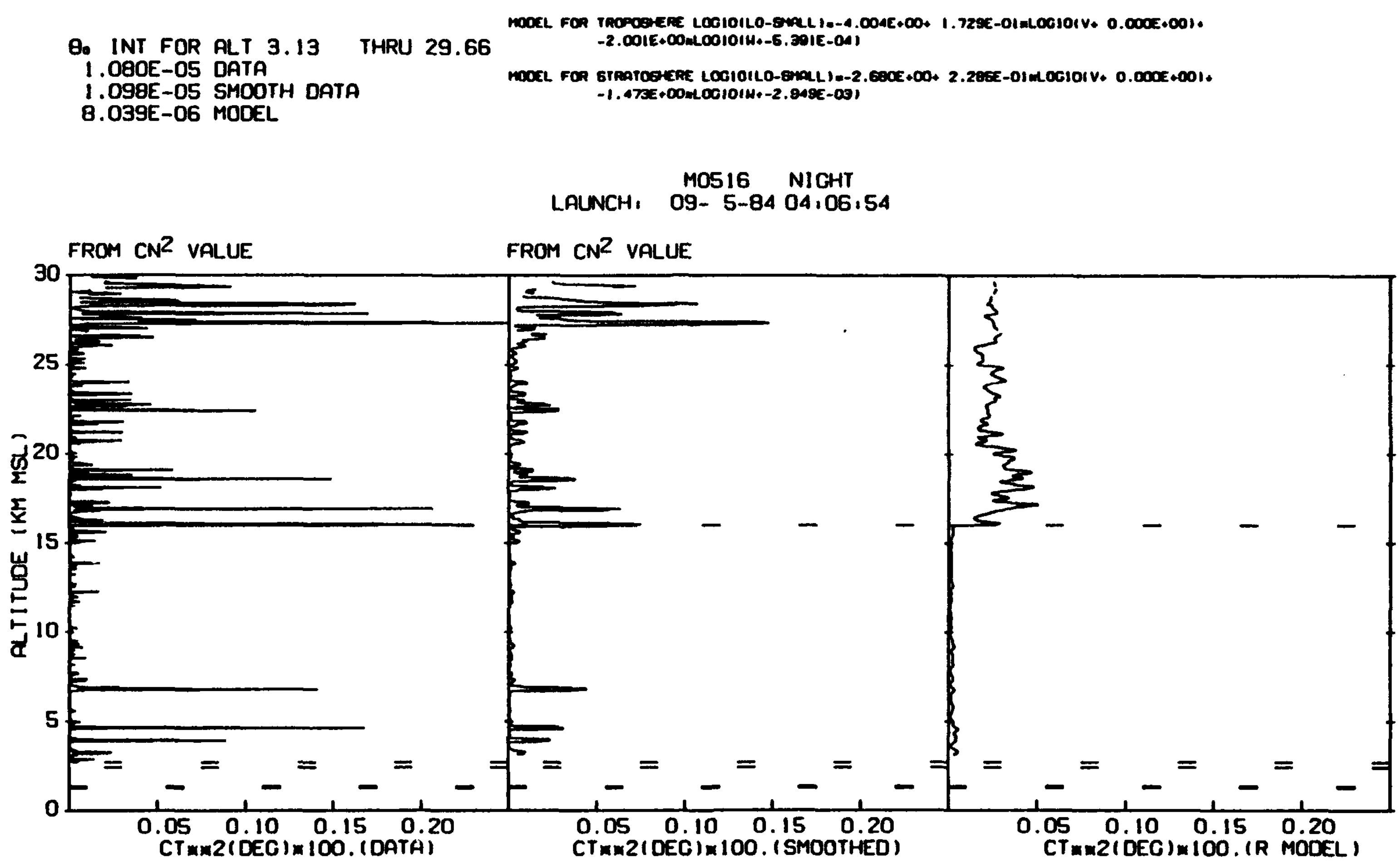

Figure 30. Same as Figure 2 but for New Mexico Flight M0516, September 1984

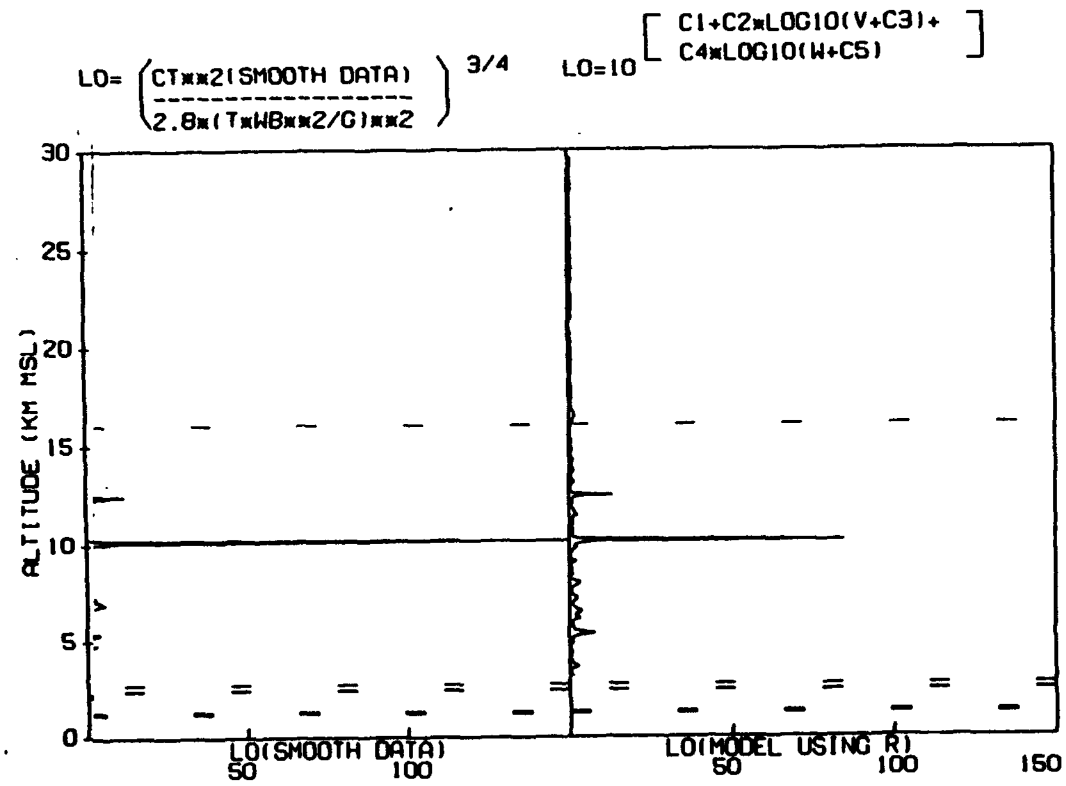

Figure 31. Same as Figure 3 but for New Mexico Flight M0516, September 1984

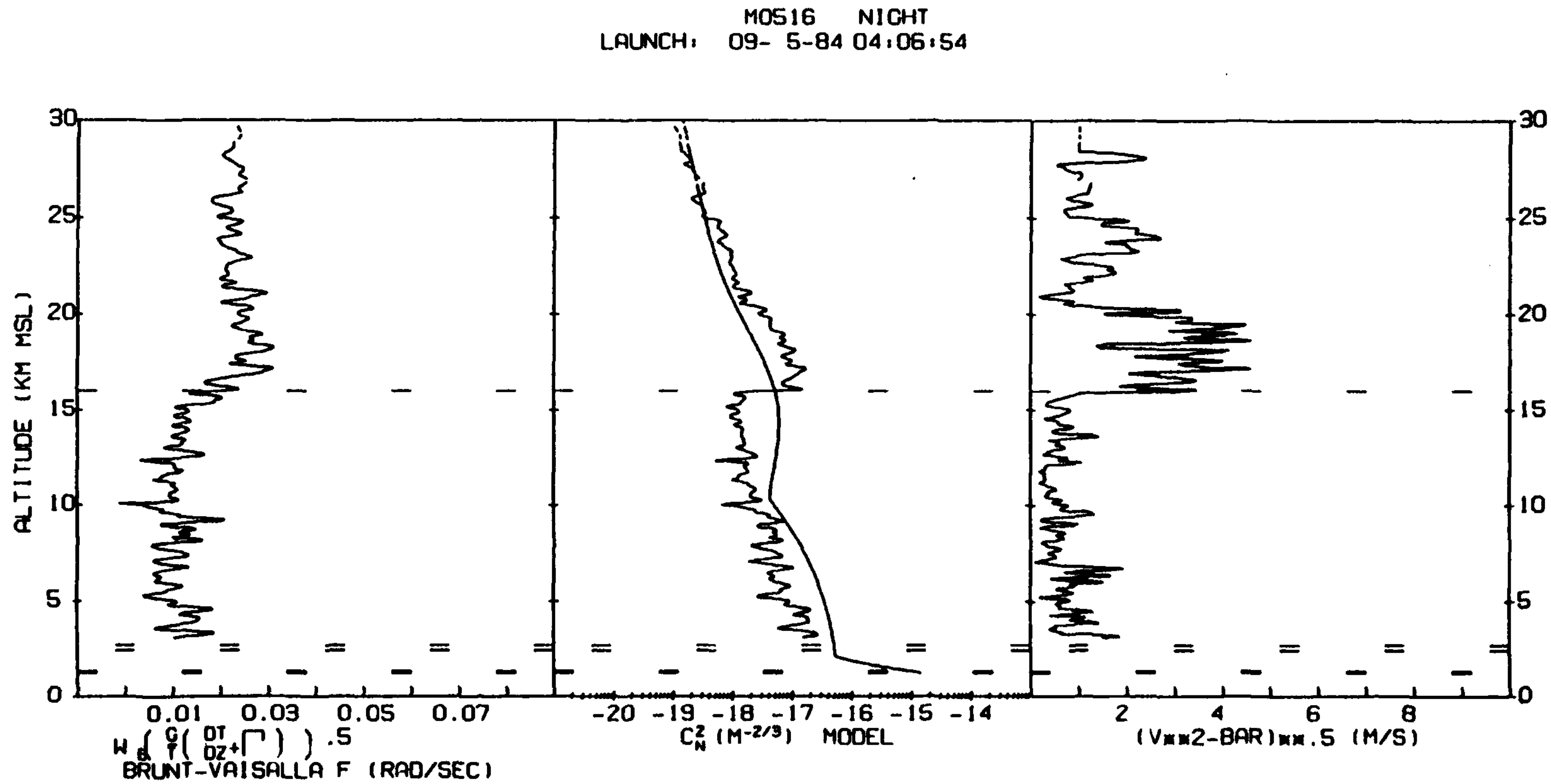

Figure 32. Same as Figure 4 but for New Mexico Flight M0516, September 1984

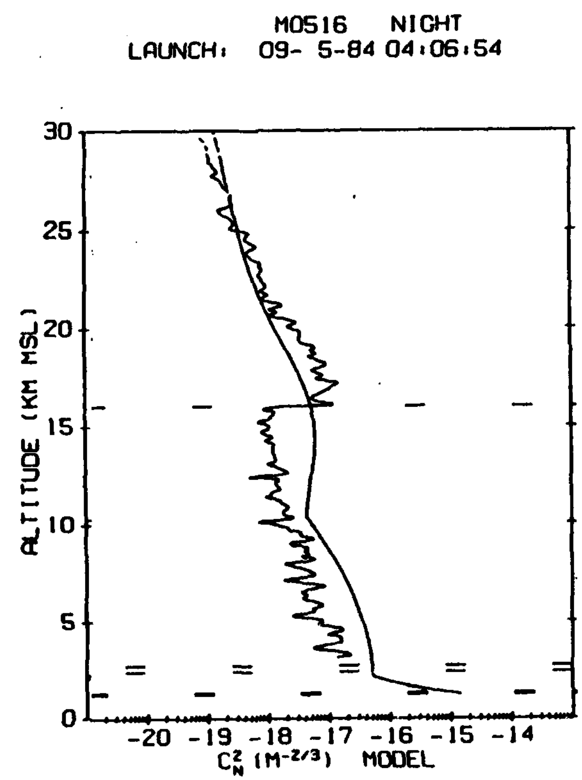

Figure 33. Same as Figure 10 but for New Mexico Flight M0516, September 1984

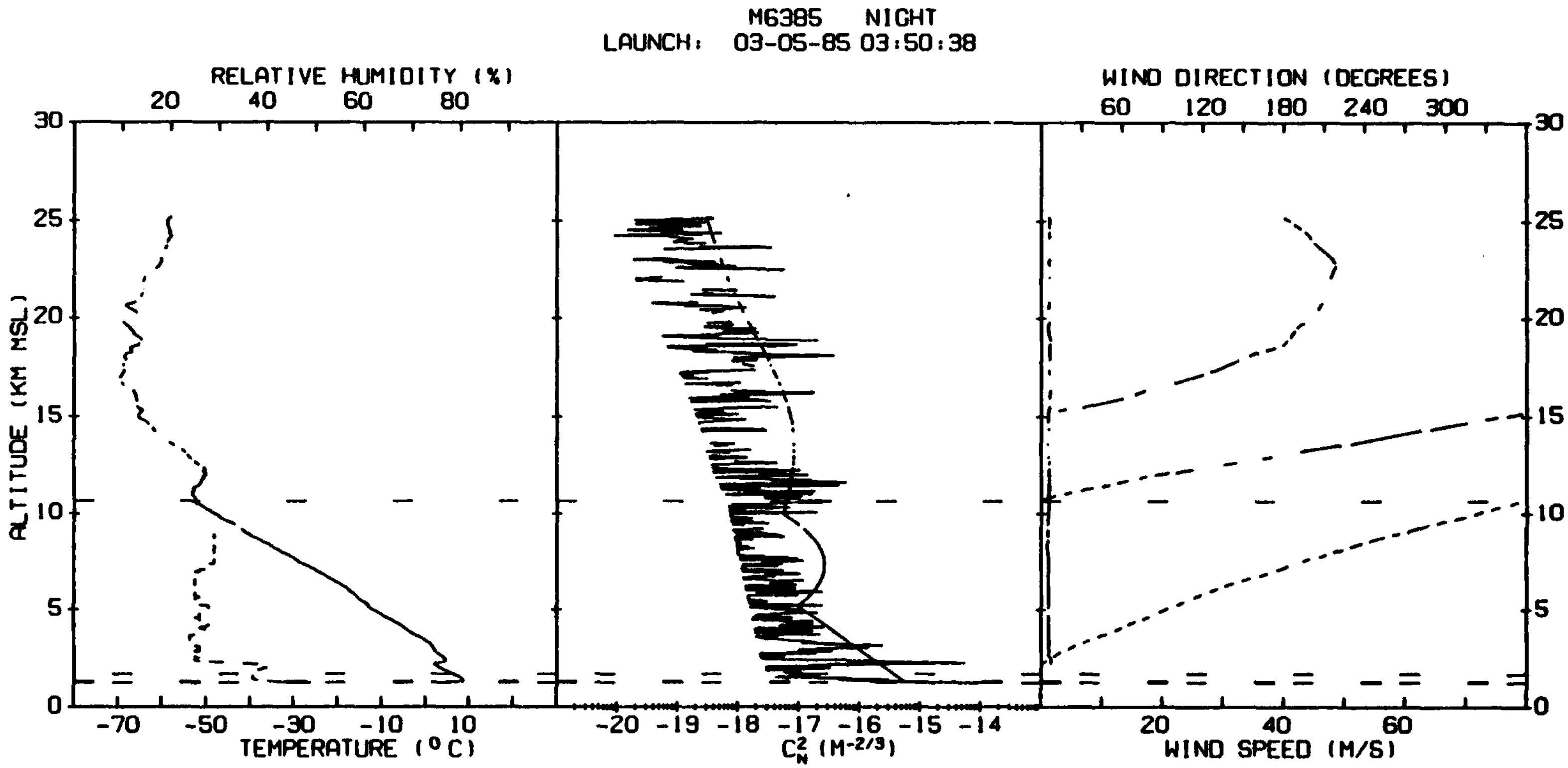

Figure 34. Same as Figure 1 but for New Mexico Flight M6385, March 1985

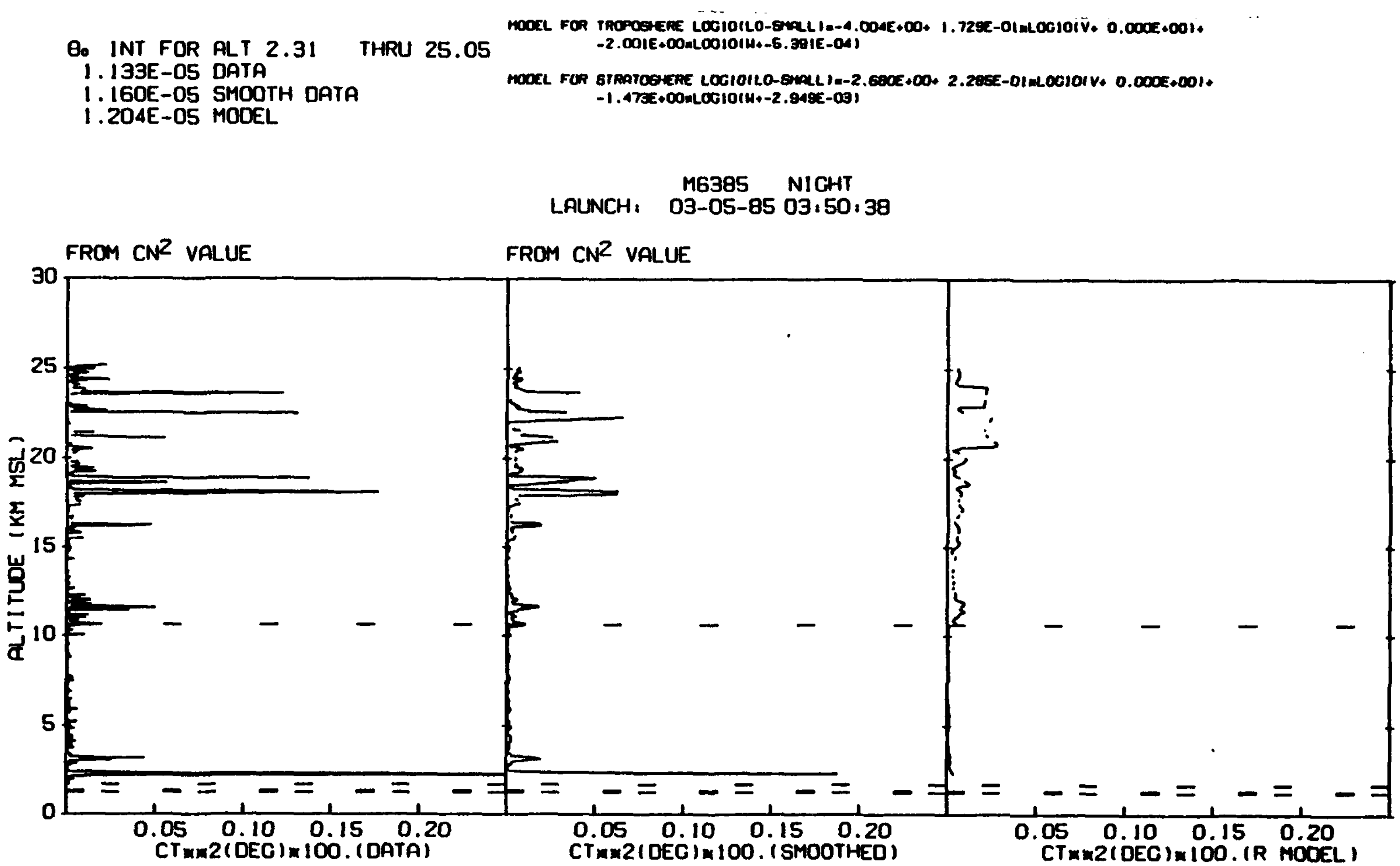

Figure 35. Same as Figure 2 but for New Mexico Flight M6385, March 1985

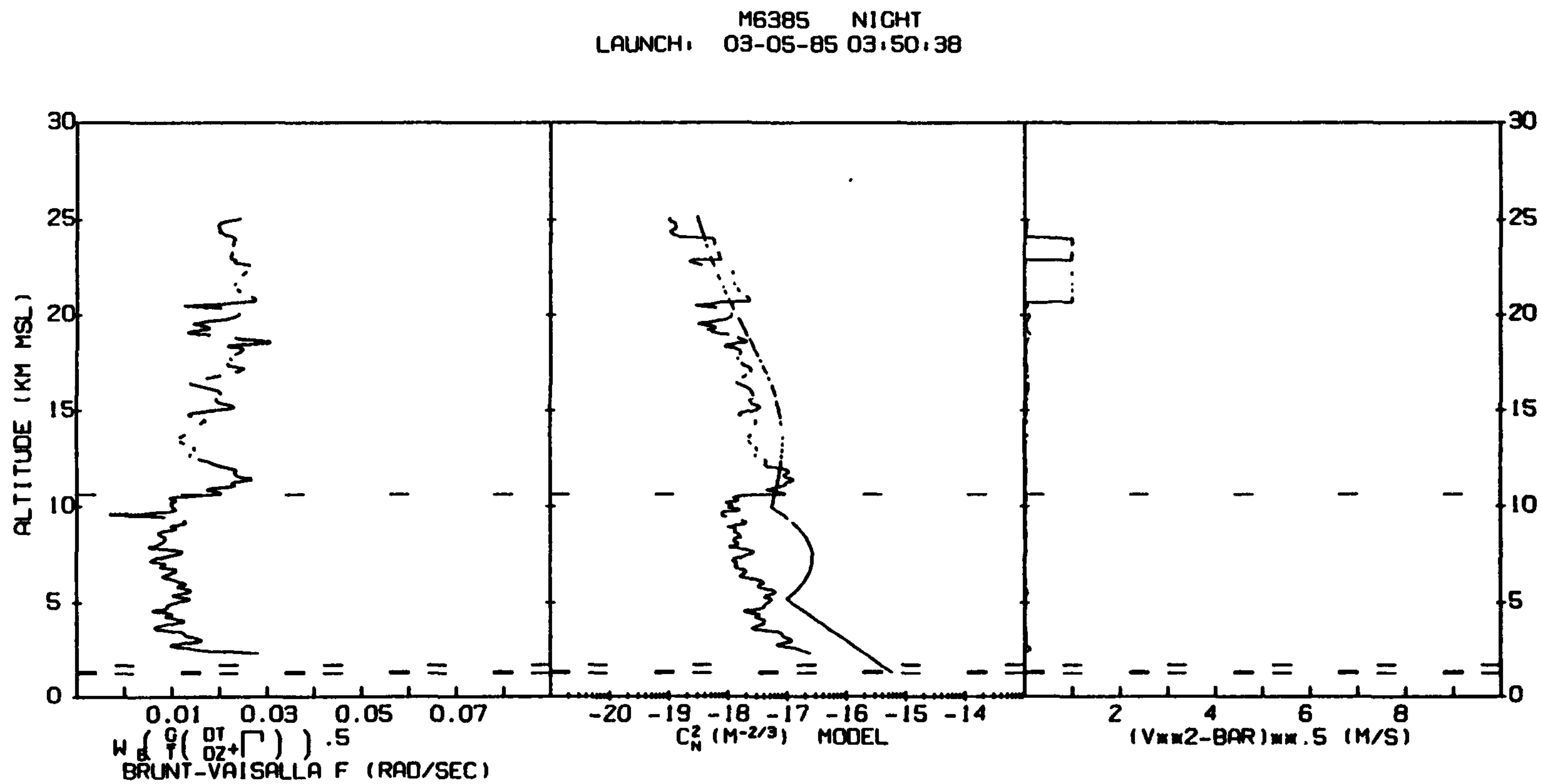

Figure 36. Same as Figure 4 but for New Mexico Flight M6385, March 1985.

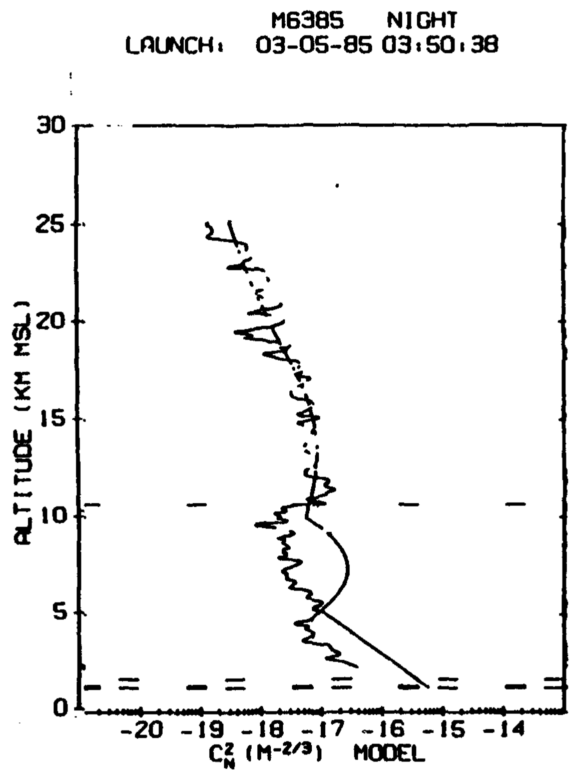

Figure 37. Same as Figure 10 but for New Mexico Flight M6385, March 1985

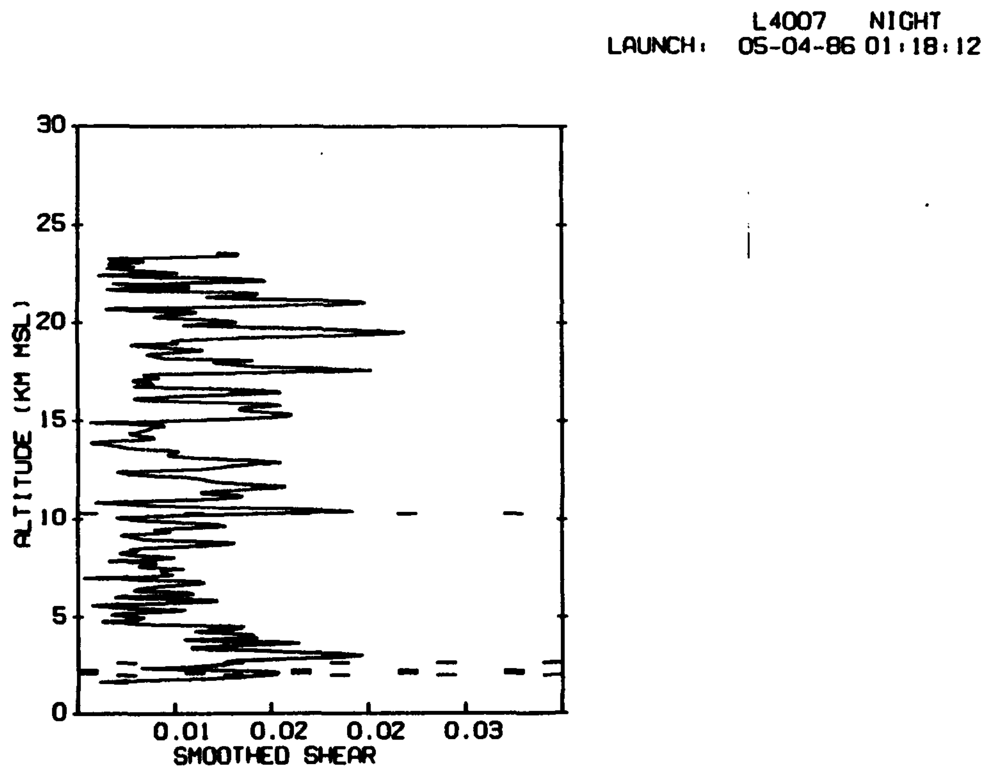

Figure 38. Smoothed 300 m Rawinsonde Shear for Pennsylvania State University Flight L4044

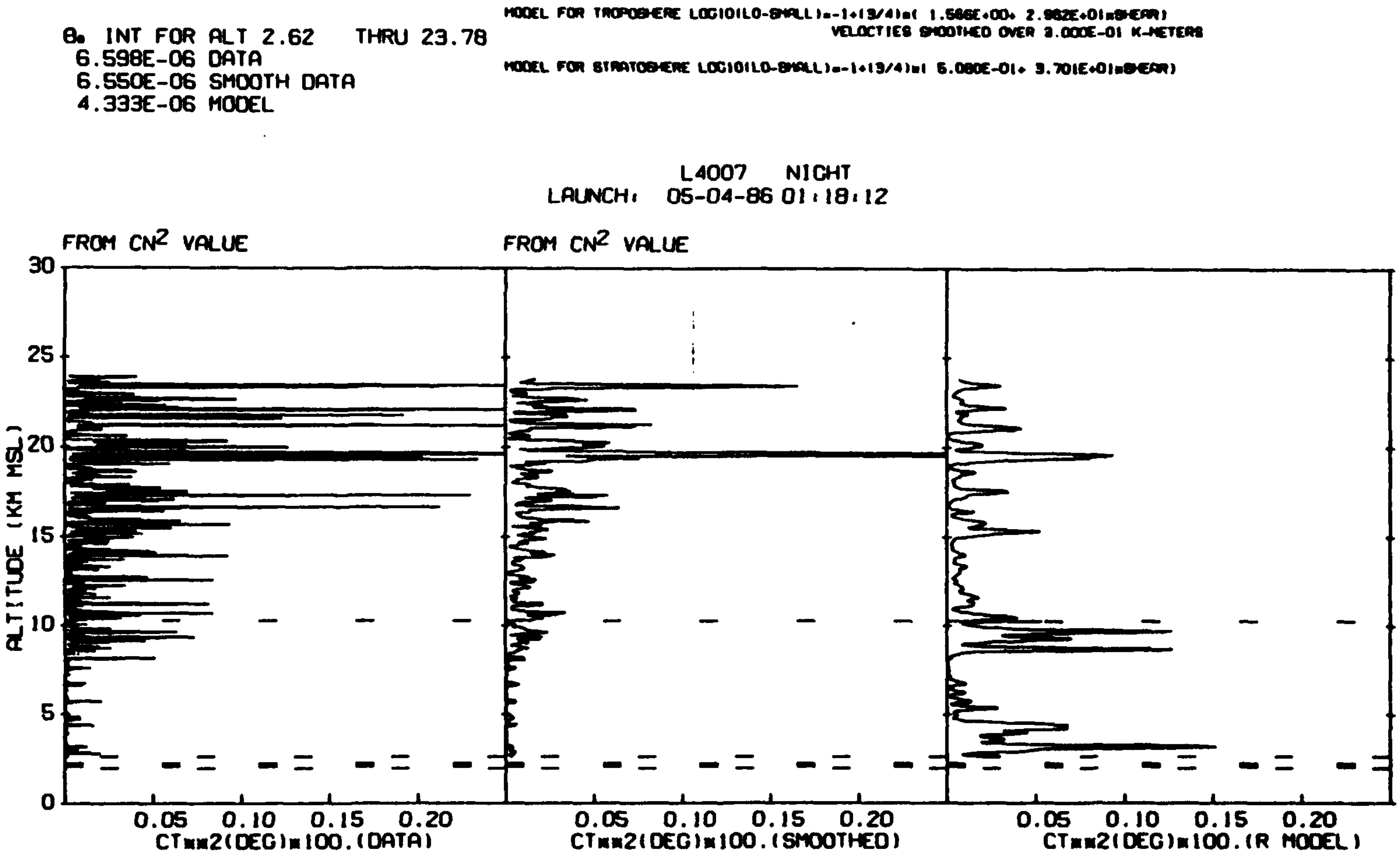

Figure 39. Thermosonde C_t^2 measurement (raw and Smoothed) Profiles Compared to Dewan, et al. C_t^2 Model Profile. Flight L4007

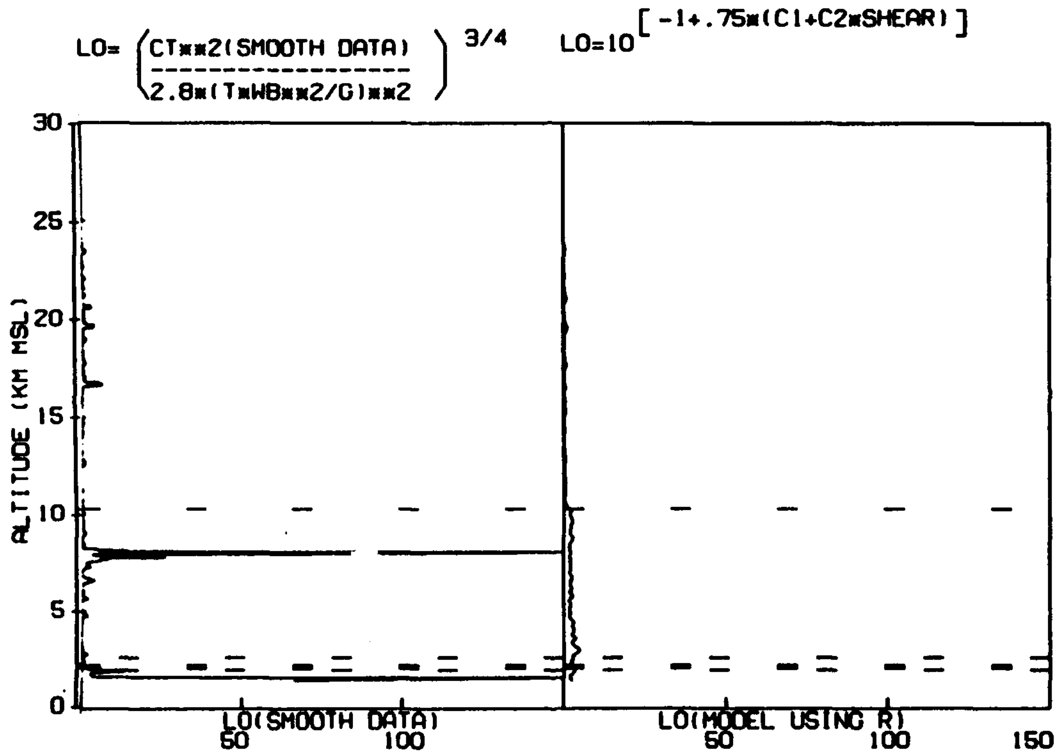

Figure 40. L(z) From Smoothed Thermosonde Data Compared to Dewan, et al. L(z) Model Profile. Flight L4007

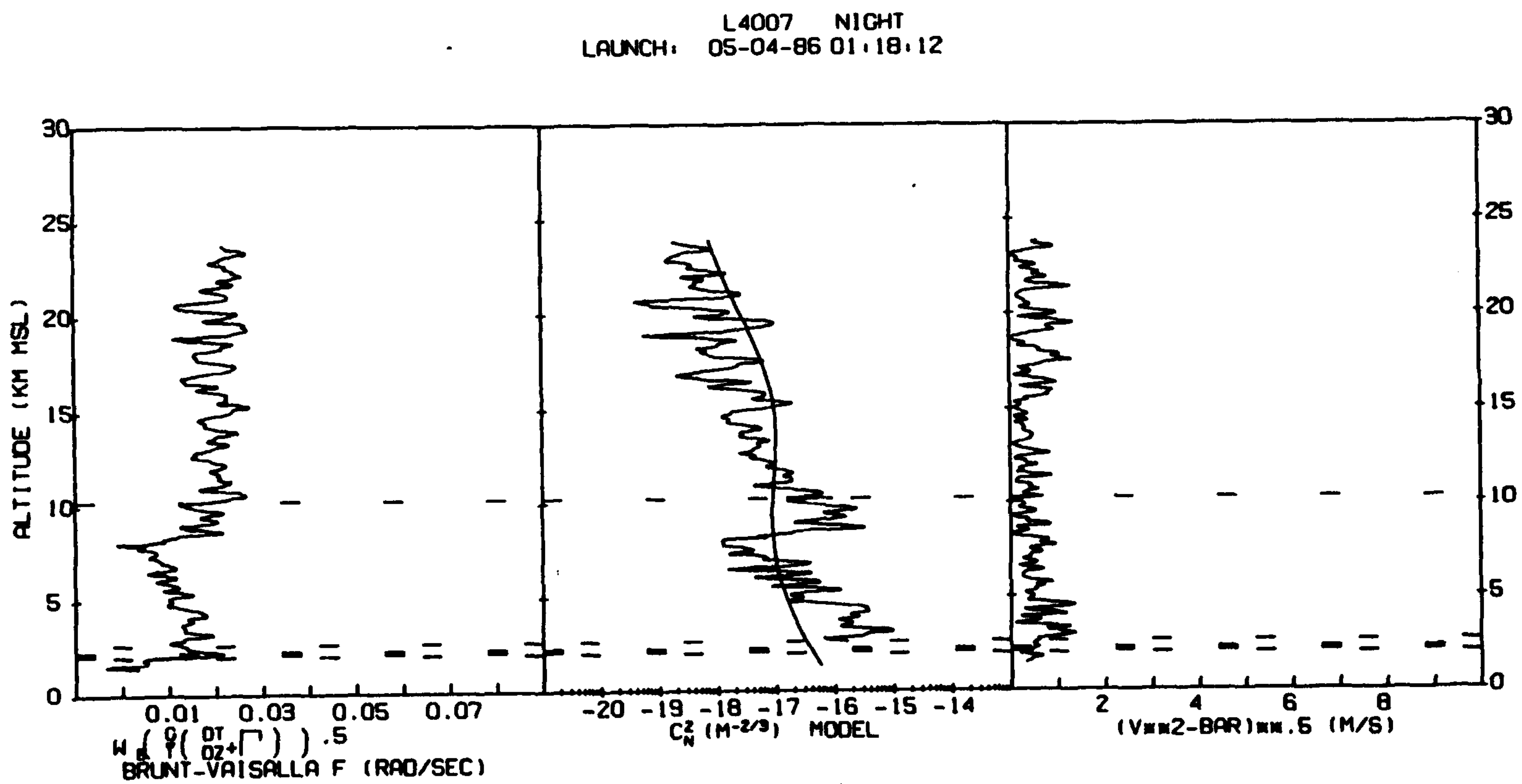

Figure 41. Brunt-Vaisala Frequency and RMS Wind Speed Profiles Derived From Smoothed Measurement Compared With Dewan et al. Model C_n^2 Profile. Flight L4007

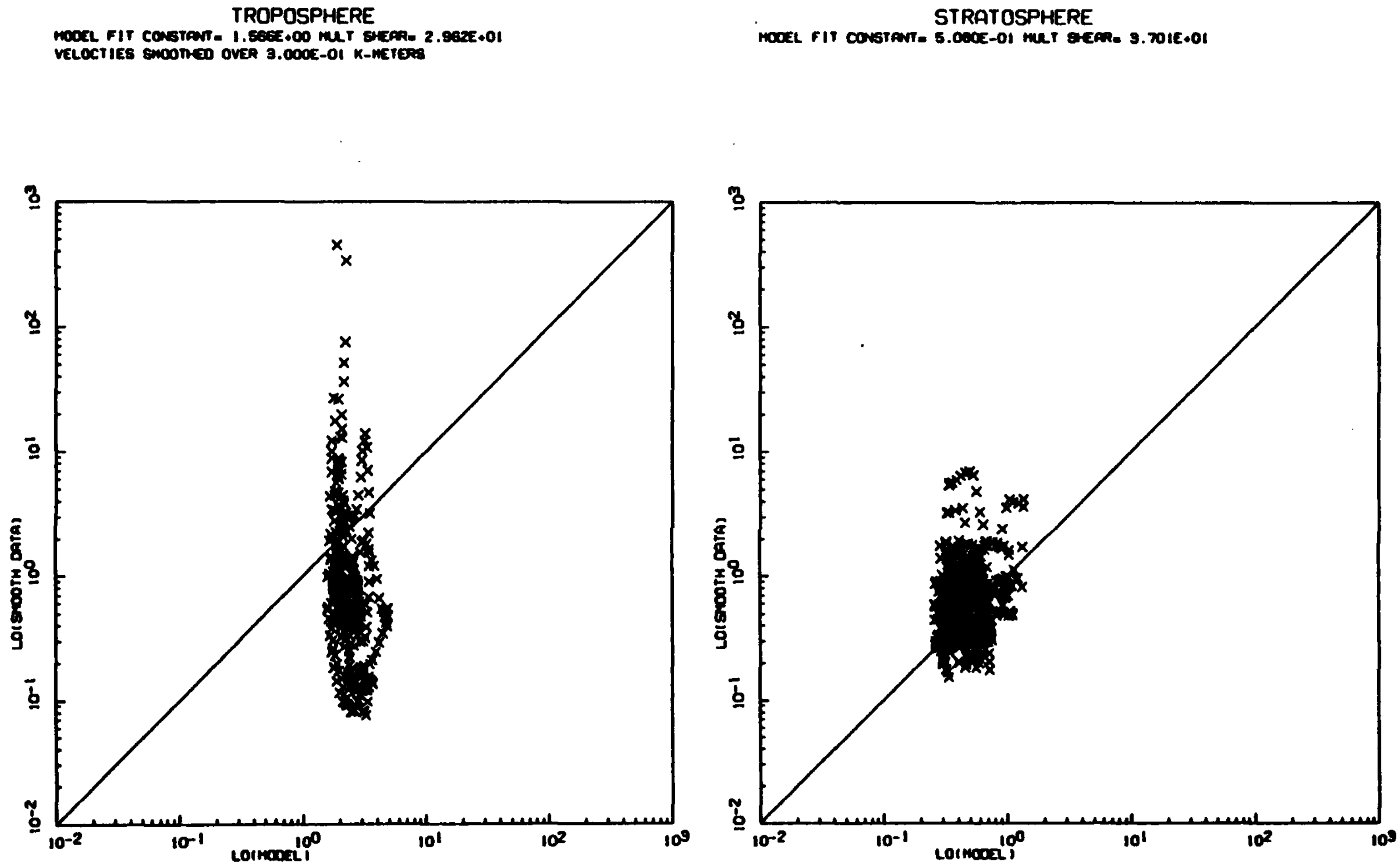

Figure 42. Scatter Plot of "L" for Smoothed Thermosonde Measurements Compared with "L" from Dewan, et al. Model. Flight L4007. Leftmost plot for troposphere. Rightmost plot for stratosphere

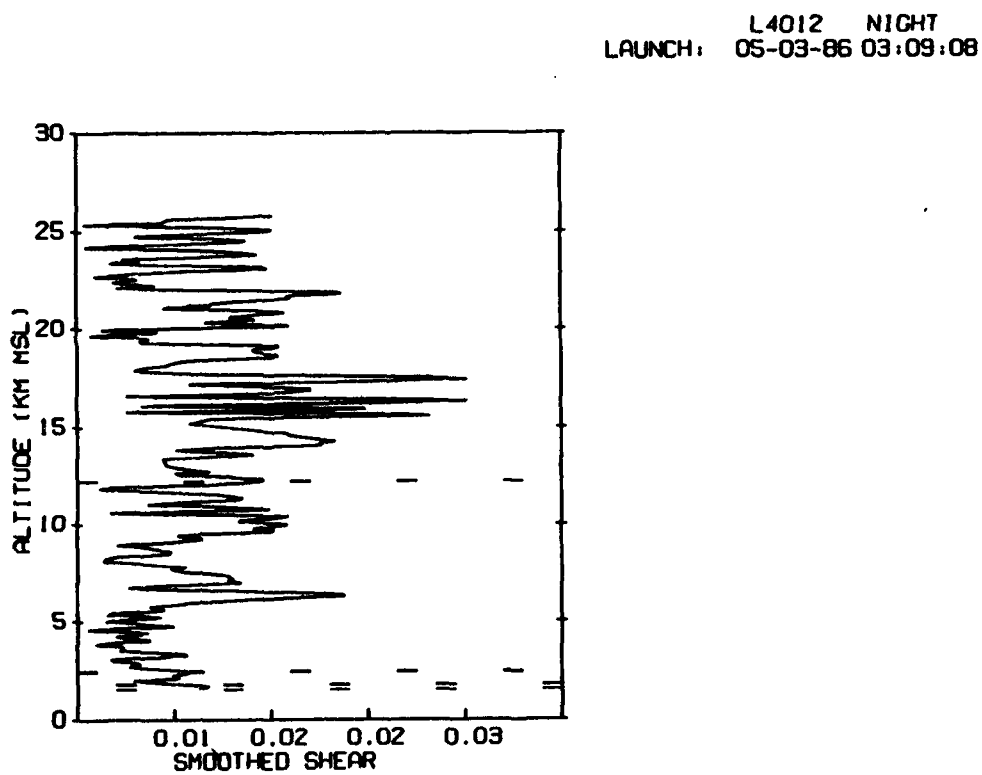

Figure 43. Same as Figure 38 but for Pennsylvania State University Flight L4012, May 1986

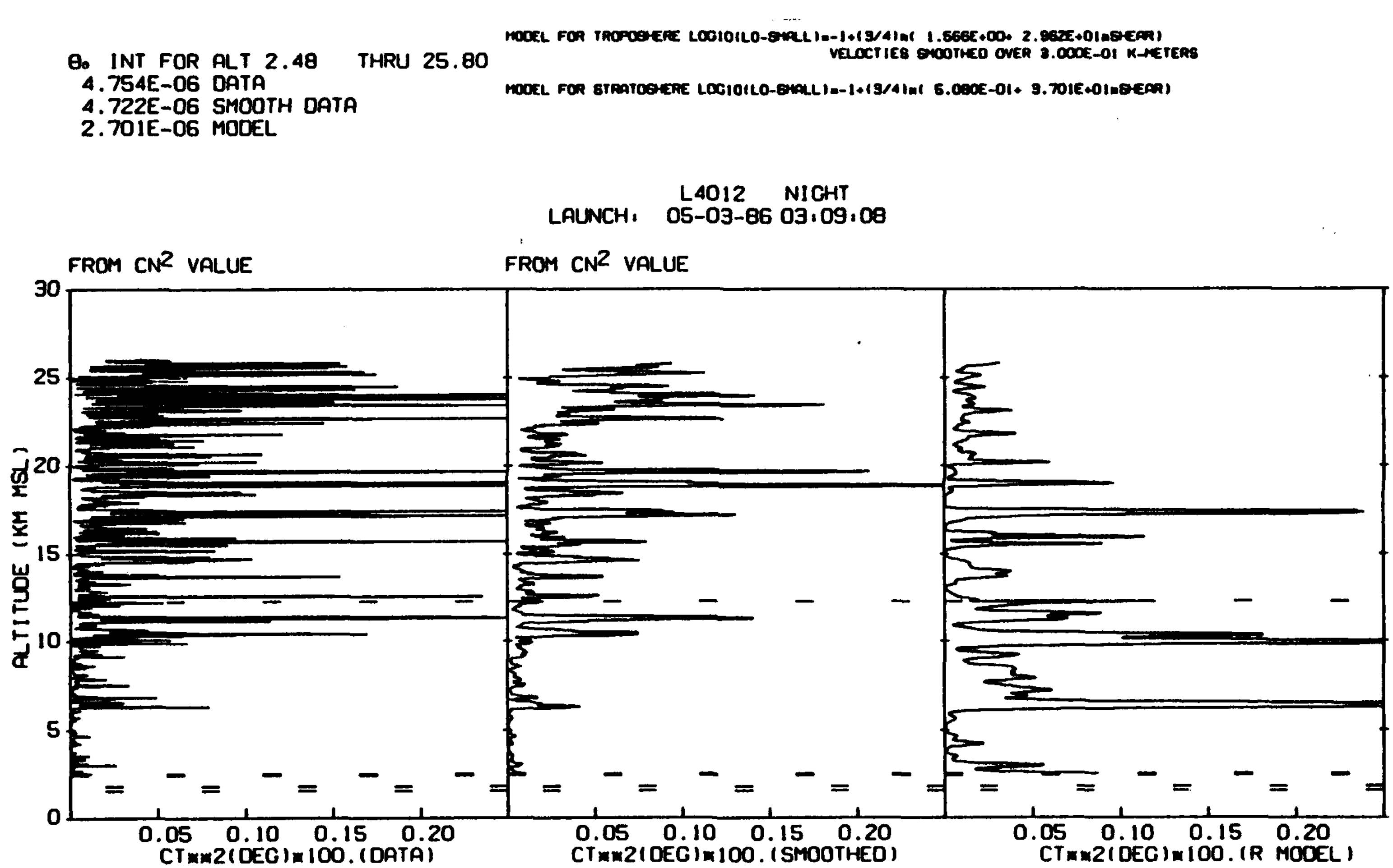

Figure 44. Same as Figure 39 but for Pennsylvania State University Flight L4012, May 1986

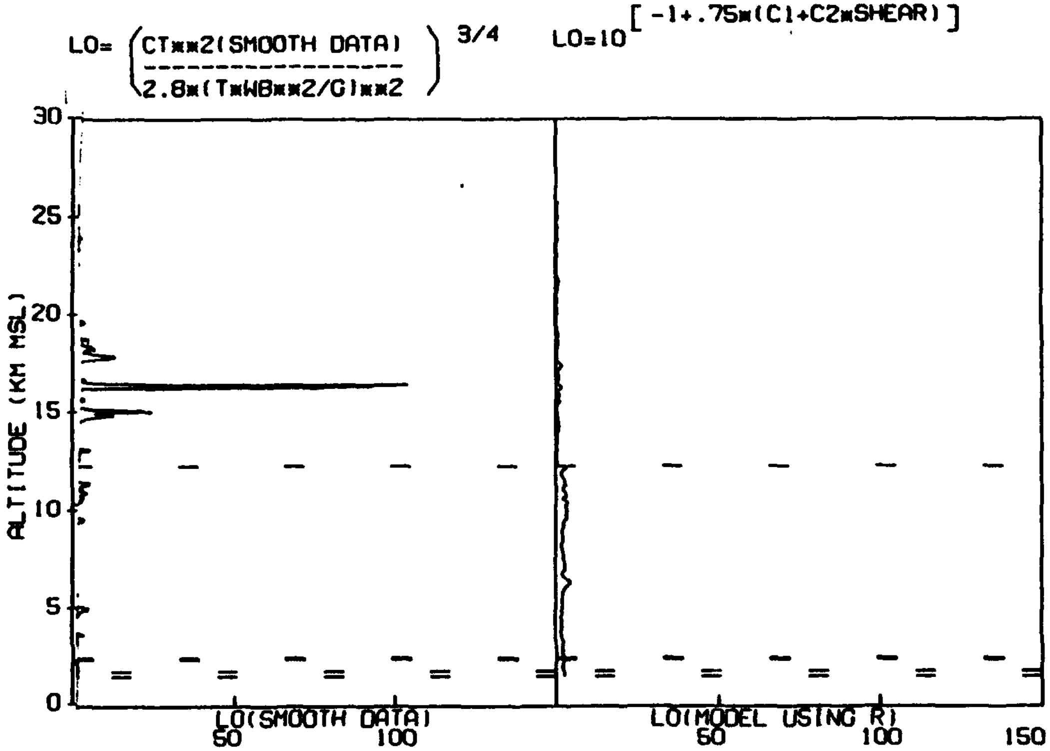

Figure 45. Same as Figure 40 but for Pennsylvania State University Flight L4012, May 1986

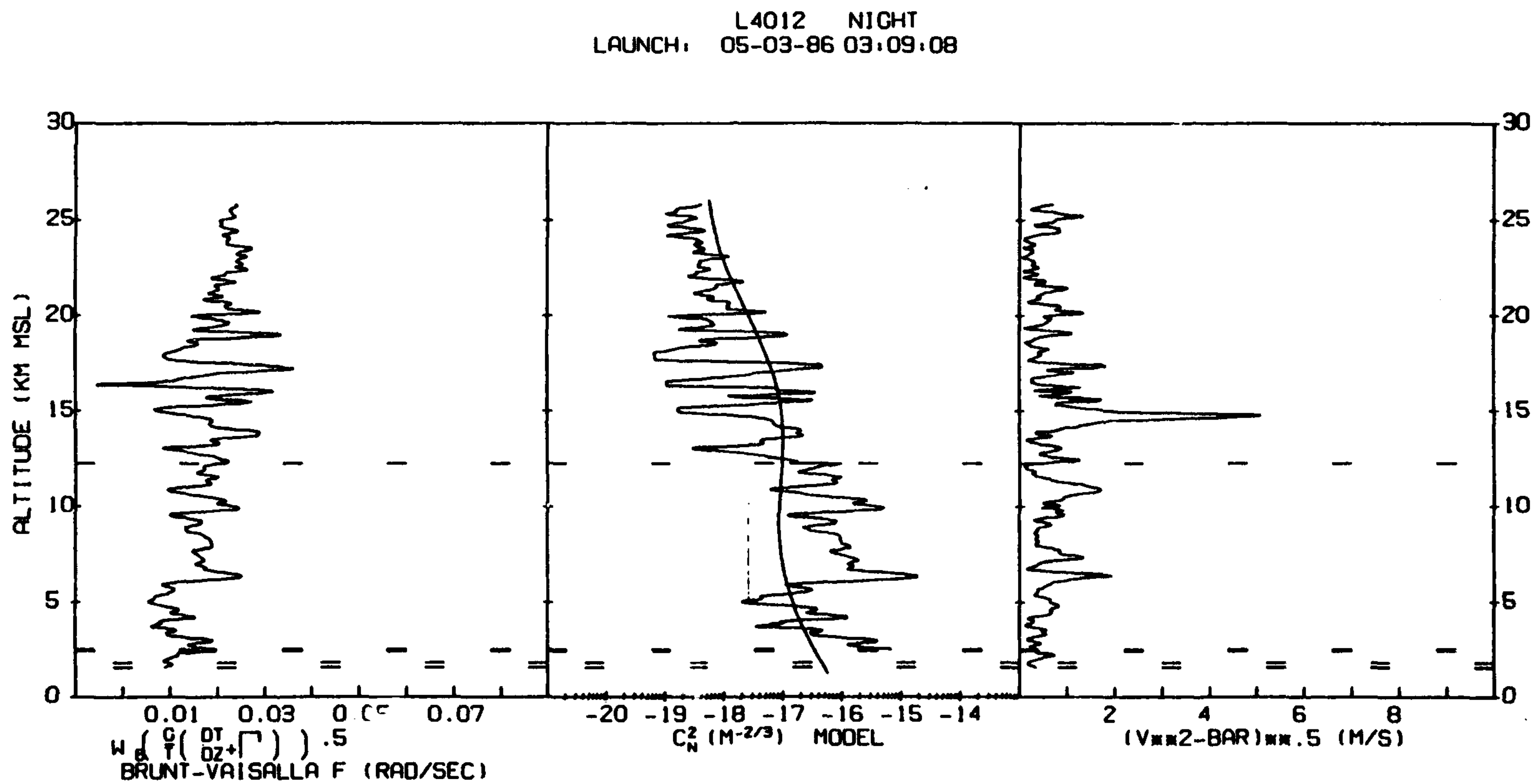

Figure 46. Same as Figure 41 but for Pennsylvania State University Flight L4012, May 1986

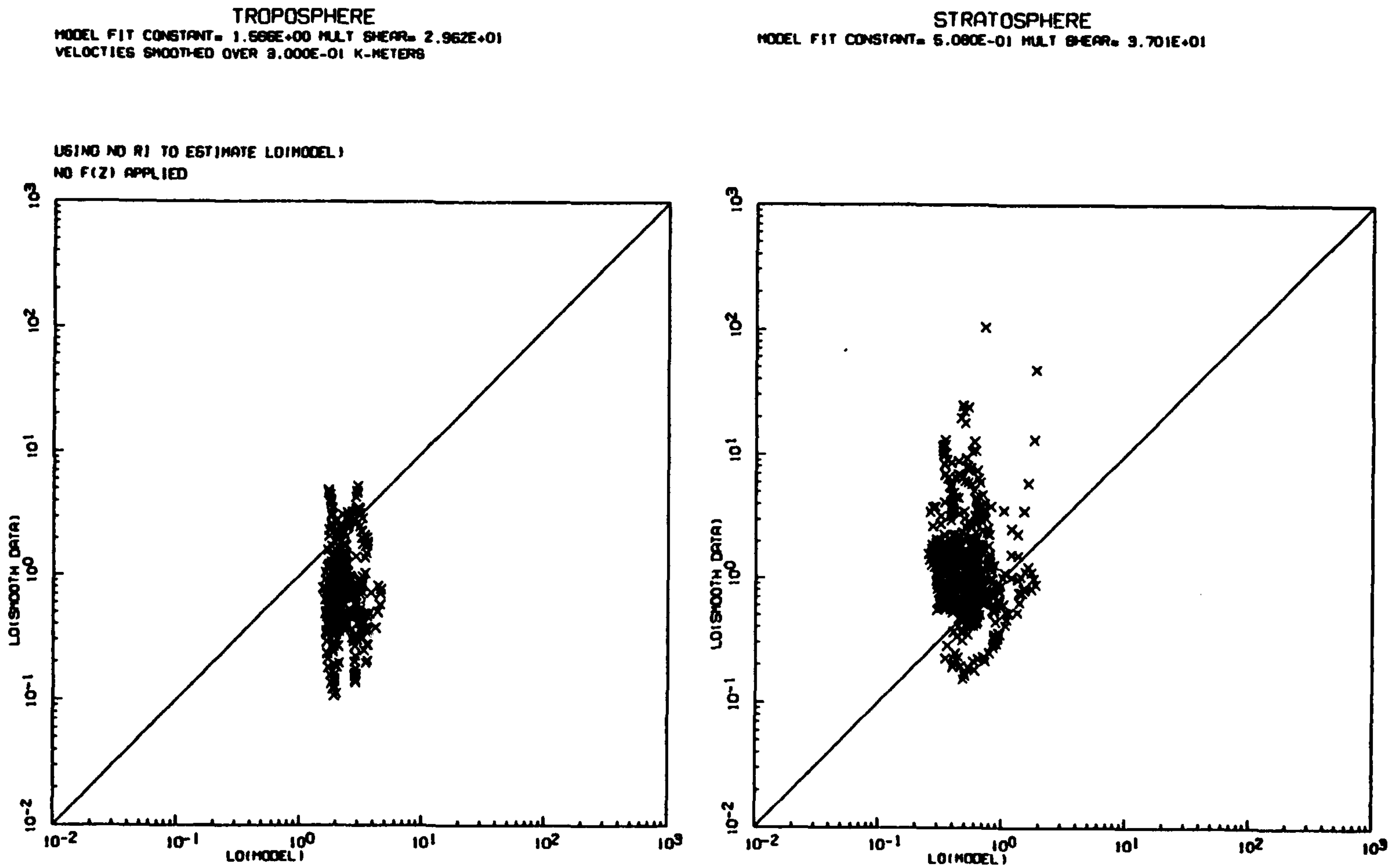

Figure 47. Same as Figure 42 but for Pennsylvania State University Flight L4012, May 1986

References

1. Brown, J. H., Good, R. E., Bench, P. M., and Faucher, G., (1982) *Sonde Experiments for Comparative Measurements of Optical Turbulence*, AFGL-TR-82-0079, ADA118740

2. Good, R. E., Beland, R. R., Murphy, E. A., Brown, J. H., and Dewan, E. M., (1988) Atmospheric Models of Optical Turbulence, SPIE V928, Modeling of the Atmosphere, Rothman, L.S. ed., pp 165-186

3. Hufnagel, R. E., (1978) Propagation through atmospheric turbulence, *The Infrared Handbook*, Wolfe, W. L. and Zississ, G. J., eds., Department of the Navy, pp 6-14

4. Warnock, J. M. and VanZandt, T. E., (1985) *A Statistical Model to Estimate The Refractivity Turbulence Structure Constant C_n^2 In Free Atmosphere*, NOAA Technical Memorandum ERL AL-10, Aeronomy Laboratory, NOAA, Environmental Research Laboratories

5. VanZandt, T. E., Gage, K. S., and Warnock, J. M. (1981) An improved model for the calculation of profiles of C_n^2 and ε in the free atmosphere from background profiles of wind, temperature, and humidity, Proc., 20th Conf. on Radar Meteorology, Nov 30-Dec 3, Boston, MA, 129-261

6. VanZandt, T. E., Green, J. L., Gage, K. S., and Clark, W. L., (1978) Vertical profiles of refractivity turbulence structure constant: comparison of observations by the Sunset radar with a new model, *Radio Science*, 13:819-829

7. Warnock, J. M., Beland, R. R., Brown, J. H., Clark, W. L., Eaton, F. D., Favier, L. D., Gage, K. S., Green, J. L., Hatch, W. H., Hines, J. R., Murphy, E. A., Nastrom, G. D., Peterson, W. A., and VanZandt, T. E., (1989) Comparison amoung clear-air radar, thermosonde and optical measurements and model estimates of C_n^2 made in very flat terrain over Illinois, *Middle Atmosphere Program Handbook*, Liu, C. H., ed., V28, June, 1989

8. Green, J. L., Beland, R. R., Brown, J. H., Clark, W. L., Eaton, F. D., Favier, L. D., Gage, K. S., Hatch, W. H., Hines, J. R., Murphy, E. A., Nastrom, G. D., Peterson, W. A., VanZandt, T. E., and Warnock, J. M., (1989) Comparisons of refractivity turbulence estimates from the Flatland VHF radar with other measurement techniques, AMS, 24th Conf on Radar Meteorol, Tallahassee, FL, March, 1989

9. Dewan, E. M., Good, R. E., Beland, R. R., and Brown, J. H., (1993) *A Model for C_n^2 (Optical Turbulence) Profiles from Radiosonde Data*, PL-TR-93-2043

10. Tatarski, V. I., (1961) *Wave Propagation in a Turbulent Medium*, McGraw-Hill

11. Govind, P. K., (1975) Omega Windfinding Systems, *J. Appl. Meteor.*, **14**:1503-1515

12. Weinstock, W. B., (1978) Vertical turbulent diffusion in a stably stratified fluid, *J. Atmos. Sci.*, **35**:1022

13. Hocking, W. K., (1985) Measurement of turbulent energy dissipation rates in the middle atmosphere by radar techniques: A review, *Radio Science*, **20**: (No. 6) 1403-1422